Crustal deformation associated with glacial fluctuations in the eastern Chugach Mountains, Alaska

Jeanne Sauber,[1] George Plafker, [2] Bruce F. Molnia, [3] and Mark A. Bryant [4]

Abstract

The changes of the solid Earth in south central Alaska in response to two major glacial fluctuations on different temporal and spatial scales have been estimated and we evaluated their influence on the stress state and ongoing tectonic deformation of the region. During the recent (1993–1995) Bering Glacier surge, a large transfer of ice from the Bagley Ice Field to the Bering Glacier terminus region occurred. We estimated the elastic displacement of the solid Earth due to ice mass redistribution from Global Positioning System (GPS) measurements at sites near the surging glacier. We can account for these displacements by transfer of an ice volume of about 14 km^3 from the surge reservoir area to the terminus region. We examined the background seismicity ($M_L \geq 2.5$) before, during, and after the surge. We found that the occurrence of small earthquakes ($M_L \leq 4.0$) in the surge reservoir region increased during the surge time interval possibly in response to a decrease in ice mass. This suggests that a small decrease in the vertical stress, σ_3, could be enough to modulate the occurrence of small, shallow earthquakes in this dominantly thrust fault setting. During this century the southern Alaska coastal glaciers have been undergoing an overall decrease in volume. Based on our compilation of changes in the extent and thickness of the coastal glaciers between the Malaspina and Bering, we calculated surface displacements due to the Earth's viscoelastic response to annual thinning and to the cumulative retreat over the last 100 years. The uplift of the region due to an average annual thinning rate of 1–6 m/yr in the ablation region is 1–12 mm/yr. For our reference model with a viscosity of 5 x 10^{19} Pa s for depths between $\approx$ 40 and 200 km the total viscoelastic response due to the retreat over the last century may be as much as a couple of meters within the coastal ablation zone near Icy Bay. The maximum decrease in σ_V between 0 and 10 km was $\approx$1.0 MPa, which is significant in relation to the stress drops in recent earthquakes ($\approx$2 to 10 MPa) but small in relation to the estimated tectonic stress magnitude. Therefore the occurrence of an earthquake such as the St. Elias (1979, $M_S = 7.2$) may have been advanced in time; however, most of the ongoing stress accumulation would be primarily due to tectonic forces.

1. Introduction

The eastern Chugach Mountain range of southern Alaska is covered with a continuous series of connected glaciers (Figure 1) [*Field*, 1975]. Although individual glacier fluctuations are variable and asynchronous, there has been a gross regional pattern of glacier retreat in southern Alaska this century [*Meier*, 1984; *Porter*, 1989; *Molnia and Post*, 1995]. By comparing the predicted elastic response of the Earth to geodetic observations, the change in ice sheet mass can be estimated [*Hager*, 1991; *Hager et al.*, 1991; *Sauber et al.*, 1995; *James and Ivins*, 1995, 1998; *Wahr et al.*, 1995]. Time-dependent deformation due to the viscoelastic response of the Earth to unloading during the last 100 years is also likely to be significant. Here we report new constraints on the retreat of coastal glaciers this century between the Malaspina and Bering Glaciers. We estimated the magnitude of viscoelastic displacements associated with this ice mass unloading and compared it with measured geodetic and longer-term deformation rates. We contrasted the importance of tectonic and glacial rebound in explaining the observed deformation rate near Icy Bay.

The recession of the Bering Glacier has been interrupted by at least six surges this century [e.g., *Molnia and Post*, 1995; *Muller and Fleisher*, 1995]. These surges involve periodic rapid movement of large quantities of ice within a glacier alternating with much longer periods of near stagnation or retreat [*Meier and Post*, 1969; *Molnia*, 1993; *Budd and McInnes*, 1974]. When a surge removes ice from the upper reaches of the glacier, its surface lowers by tens or hundreds of meters as ice is transported down glacier, where the ice thickens. Sometimes this is accompanied by an advance of the glacier terminus. The ice mass changes result in uplift of the solid Earth near the unloading (surge reservoir region) and subsidence beneath and near the receiving area [*Cohen*, 1993; *Sauber et al.*, 1995]. In this paper we employ precise geodetic measurements made with the Global Positioning System (GPS) at sites adjacent to the Bagley Ice Field and near the Bering Glacier (Figure 1) to supplement glaciological data to constrain ice mass redistribution, to estimate the total ice mass transfer and to explore the implications of our results for understanding the surge cycle of the Bering Glacier.

The predicted stress changes associated with the Bering Glacier surge and glacier retreat in the last 100 years are small in comparison with the tectonic stress levels estimated from borehole breakout data at a comparable depth. Based on earlier (water) reservoir-induced earthquake studies, however, we postulated that the small stress changes associated with glacial fluctuations this century could exert discernible control on the occurrence of earthquakes. Seismicity ($M_L \geq 2.5$) bracketing the time of the Bering Glacier surge and the location of moderate to large earthquakes ($M_L \geq 4.0$) between 1973 and 1997 were examined to evaluate whether glacial fluctuations had discernible influence on earthquake occurrence.

2. Representation of the Crust and Upper Mantle Rheological Properties for Estimating Surface Deformation

The specific response of the Earth to a change in surface load across different spatial scales (10^0–10^4 km) and on a variable time scale (10^0–10^4 years) depends on the rheological structure of the crust and mantle. The surface displacements associated with the recession of continental scale ice sheets [e.g., *Peltier and Andrews*, 1976], other Alaska glaciers, [e.g., *Clark*, 1977], and lake loads [e.g., *Bills et al.*, 1994] have been used both to probe Earth rheology and to provide constraints on the unloading history.

As was summarized by *Kirby* [1985], the thick and mechanically heterogeneous continental crust presumably plays an active role in determining the style of near-surface deformation. In addition, mobile aqueous fluids are thought to play a major role, via pore pressure effects on brittle materials, in controlling rock strength of the shallow and midcontinental crust. The gradual transition from localized deformation along faults or fractures to distributed strain within the crust is thought to occur above a certain temperature, but the ratio of the least compressive stress (σ_3) to the differential stress ($\sigma = \sigma_1 - \sigma_3$) also is hypothesized to play an important role.

In this study we calculated the response of the Earth to two glacial fluctuations. The Bering Glacier surge caused large localized surface changes over the time interval of 2 years. Since the spatial scale of the ice thickness changes is less than 30 km^2, the crust will deform primarily elastically and little viscous deformation is assumed to occur. The representation of Earth rheology that we used to calculate surface displacement was a layered elastic model, and the geometrical complexity of the load changes were represented by disks with a diameter of 5 km.

For ice thickness changes over the wider region as-

sociated with glacial retreat in the last 100 years, the viscoelastic response of the upper mantle, and possibly the lower crust, needed to be calculated. Whether the upper mantle is best represented as a Newtonian or non-Newtonian fluid depends on the dominant deformation mechanism [*Karato and Wu*, 1993]. Here the Earth's response to a load-induced perturbation to ongoing tectonic processes is represented, and we assumed a linear viscous rheology. The lower crust and the upper mantle have effective viscosities that have been estimated to range from 10^{18} to 10^{22} Pa s with Maxwell times (ratio of viscosity to shear modulus) of months to thousands of years.

Lateral asthenospheric viscosity variations would presumably play an important role in calculations of deformation rates [*Kaufman and Wu*, 1998]. Thus we used a finite element model with a subducting slab [after *Cohen*, 1996] to represent the complex rheological structure at this plate boundary. Additionally, different glaciers between the Malaspina and Bering have variable retreat profiles. In this study, the viscoelastic response of the Earth was calculated for a general two-dimensional retreat profile. The range of viscosity values tried was derived from work on postseismic deformation in Alaska and lake and glacial unloading studies.

3. Global Positioning System

During June of 1993 and 1995, GPS measurements were made at the sites shown in Figure 1 for 1–12 days. In 1997, only the coastal sites between Icy Bay and the Bering Glacier were observed (Table 1). Most daily observing periods were greater than 8 hours. GAMIT software [*King and Bock*, 1997] and GPS phase observations were used to estimate station coordinates, orbit, Earth orientation, and atmospheric parameters each day as described by *Feigl et al.*[1993]. We then used the GLOBK software [*Herring*, 1997] to estimate station coordinates and a velocity over some time period by combining these estimates and their covariance matrices with those from a similar analysis performed at the Scripps Orbital and Permanent Array Center (SOPAC) [*Fang and Bock*, 1995] using observations from 30-60 stations of the global tracking network coordinated by the International GPS Service (IGS) for Geodynamics. The reference frame was defined by minimizing the adjustments in velocities of 12 IGS stations, including Fairbanks, from their values in the North American fixed International Terrestrial Reference Frame (ITRF96) [*Boucher et al.*, 1996].

The horizontal velocities of the stations from our study region are given in Table 1 in a North American frame, obtained by rotating from the no-net-rotation frame of ITRF96 to North America using the NUVEL-1A global plate model [*DeMets et al.*, 1994]. This reference frame is most useful for comparing a tectonic model of ongoing deformation to our geodetic observations. The vertical velocities are given, however, relative to Cape Yakataga to provide a regional reference frame. Of the sites given in Figure 1, Cape Yakataga is furthest from ice fluctuations, and the predicted tectonic uplift is small (±5 mm/yr or less). In a study of earlier GPS results which included data for 1993 and 1995 [*Sauber et al.*, 1997], we suggested that the daily scatter in horizontal position estimates from an individual survey fails by a factor of about 2 to account for the errors with correlation times of several years. Based on an analysis of the daily position of globally distributed continuous GPS data, *Mao et al.* [1999] suggest that the formal error in the vertical component may be underestimated by a factor of 5 or greater. In this study the daily vertical repeatabilities show greater scatter than the horizontal components; so the formal errors have been scaled by a factor of 3.

4. Tectonic Strain Accumulation

In our study region, tectonic strain accumulation is due primarily to subduction of the Pacific plate and collision of the Yakutat terrane with interior Alaska [e.g., *Plafker et al.*, 1994]. In this geologically complex region between the transcurrent Fairweather fault and the Alaska-Aleutian subduction zone, recent crustal shortening and strike-slip faulting occurs offshore in the Gulf of Alaska (1987-1988, $M_S = 6.9, 7.6, 7.6$) and onshore in the Chugach-St. Elias Mountains (1979, $M_S = 7.2$). Prior great earthquakes in the region occurred in 1899 ($M_W = 8.1$, Yakataga; $M_W = 8.1$, Yakutat Bay) [*Thatcher and Plafker*, 1977, unpublished manuscript, 1977].

The tectonic process assumed to exert the greatest influence on the geodetic observations reported in this study is deformation associated with a locked plate interface at shallow depths (≤40 km) [*Savage and Lisowksi*, 1988]. The horizontal rate of deformation at stations located more than 20 km from major glacial fluctuations are consistent with the deformation rate predicted from elastic dislocation models of a locked main thrust zone [*Sauber et al.*, 1997]. Of the stations given in Figure 1 and Table 1, only the Yakataga sta-

tions (VYAK, YAKU, FURR) and, to a lesser extent, TIME were used to constrain interseismic strain accumulation models. Relative to stable North America the horizontal rates of tectonic deformation across the region given in Figure 1 are predicted to be 20–40 mm/yr, and the estimated tectonic uplift rates range from approximately zero near the Gulf of Alaska coast up to 12 mm/yr further inland.

5. Crustal Deformation in the Region Near the Surge of the Bering Glacier

The GPS-derived displacement between 1993 and 1995 reflects crustal deformation due to tectonic and nontectonic forces. In the previous section we discussed the predicted short-term tectonic strain, and in this section we discuss the crustal deformation due to large changes in ice thickness as a result of the 1993–1995 glacier surge. The GPS measurements cannot be used to uniquely constrain both the location and magnitude of ice thickness changes. Therefore glaciological data were used to estimate the general region that underwent ice thickness changes, as well as to provide some constraints on the relative magnitude of these changes (Plate 1). The GPS results were then used to test alternate ice transfer models suggested from the glaciological data. Our initial ice change model prompted us to make an aircraft flight over the surge reservoir region (B. Molnia, August 1999). We were able to identify trimlines, especially on south and east facing slopes (for example, near station Isle, Plate 2), associated with ice thinning attributed primarily to the surge.

5.1. Glaciological Constraints on Transfer of Ice Mass During a Surge

The results of an extensive effort to study the 1993–1995 Bering Glacier surge have provided some constraints on its timing, spatial extent, and ice thickness changes [*Lingle et al.*, 1993; *Molnia*, 1993; *Molnia et al.*, 1994; *Molnia and Post*, 1995; *Roush*, 1996; *Herzfeld and Mayer*, 1997; *Fatland*, 1998]. The surge seems to have originated south of the equilibrium line in the spring of 1993. Rapid ice movement down-glacier into the piedmont lobe and up-glacier into the Bagley Ice Field followed [*Lingle et al.*, 1993; *Fatland*, 1998]. By late in the summer of 1993 the terminus began to advance. Ice transfer to the receiving area resulted in terminus advance of about 5 km along its 30-km-wide front [*Krimmel*, 1994], and parts of the terminus advanced approximately 9 km [*Molnia et al.*, 1994].

Fatland and Lingle [1998] and *Fatland* [1998] used Cband synthetic aperture radar (SAR) interferometry to estimate surface ice velocities on the Bagley Ice Field prior to and during the surge. Their studies documented regions of fast moving ice in the eastern and western Bagley Ice Field that extended up to elevations of about 1500 m. Additionally, aircraft flights over the region provided some constraints. Stranded snow on the valley wall 25–100 m above the drawdown of the lower Bagley Ice Field suggested extensive lowering (B. Molnia, field observations, 1993, 1994). In August 1999 we took photographs and videotaped the ice margin during a fixed wing aircraft flight over the portion of the glacier involved in the 1993–1995 surge (B. Molnia, 1999). For example, the changes shown by Plate 2 reflect the cumulative thinning due primarily to the surge as well as annual thinning in the ablation zone.

5.2. Model of Ice Thickness Changes

On the basis of glaciological field observations, we identified the general region that underwent thinning. We specified vertical ice lowering in the surge reservoir over a broad region between elevations of ≈900 m on the upper reaches of the Bering Glacier and ≈1500 m on the Bagley Ice Field. On the basis of ice velocities during the surge we created a general relative unloading model. Specifically, ERS1 synthetic aperture radar data from the winter of 1994 were used by *Fatland* [1998] to estimate surface, horizontal ice velocities of 0.3 m/d in the eastern Bagley Ice Field at elevations of ≈1500 m and up to 4.5 m/d in the Bagley Ice Field near the top of the Bering Glacier at ≈1220 m. The region with fast moving ice during the surge was at elevations below the equilibrium line altitude (ELA). We assumed the region of greatest extension and thinning is associated with the highest surge ice velocities in the reservoir region, and we tapered the thickness change to zero at the limit of fast moving ice (Figure 19 of *Fatland* [1998]).

This unloading model included both surge-related ice thinning and annual thinning associated with retreat. Near the Tana Glacier, retreat of the glacier is the primary source of ice thinning. For other parts of the ice thinning region given in Plate 1 the annual thinning is as much as an order of magnitude smaller than the surge change. The value assumed for the initial unloading model over the 1993–1995 time interval shown in Plate 1 is given from top left to bottom right in meters: -15, -15, -10, -30, -45, -45, -30, -30, -15, -5,

-5, -5, -35, -35, -10, -20, -15, -5, -15, -15, -10, -10, -5.

The magnitude of ice thickening during the surge was greatest in the region in which the glacier advanced (Plate 1). Additionally, thickening of the Bering Glacier piedmont lobe was estimated to be 40–150 m with mobile bulges exceeding 200 m in thickness [*Roush*, 1996; B. Molnia, field observations, 1993–1996]. We used ERS1 data from the Bering Glacier piedmont lobe to identify regions of ice advance and thickening (presurge position definition is from images on June 16, 1992, and April 20, 1993; postsurge, from a September 22, 1995, image).

Since the water load associated with Vitus Lake (northwest of the station DON) was replaced by a thicker ice load, we did place some disks in this region, but we made them thinner than the disks due north and northeast of the station DON. Unfortunately, we had just one geodetic station in this region, and we are unsure of the reliability of the displacement for estimating ice load changes; other processes such as sediment loading offshore due to the high flux of sediments associated with the surge could have been important as well.

An initial relative model of ice loading is given from top left to bottom right in meters: 10, 10, 10, 10, 10, 10, 10, 10, 10, 10, 30, 30, 45, 40, 50, 50, 50.

We made the simplifying assumption that the ice volume removed ($\mathbf{L}^-$) during 1993–1995 surge is approximately equal to the ice volume added ($\mathbf{L}^+$) to the Bering Glacier piedmont lobe. That is, $\sum_{i=1}^{21} L_i^- = \sum_{j=1}^{17} L_j^+$, where $L = \rho_{ice} \times H$, ρ_{ice} equals the density of ice, H corresponds to the ice thickness due to the surge (red only; black in the plate is attributed primarily to annual retreat of the Tana) change over a given time period, i equals the number of disk loads to represent the change in ice thickness in the Bagley Ice Field and upper reaches of the Bering Glacier, and j equals the number in the Bering Glacier piedmont lobe (Plate 1, blue values). This assumption is supported by observations of ice transfer during other surges in Alaska and in the Pamirs of Asia [*Dolgushin and Osipova*, 1975; *Kamb et al.*, 1985].

5.3. Elastic Displacements Caused by Redistribution of Ice Mass

For an individual disk load (L_i) of density ρ_{ice} and radius α, the vertical (u_i) and horizontal (v_i) displacement as a function of distance from the center of a disk are given in terms of hypergeometric functions by equations 12–16 of *Farrell* [1972]. We assumed that the instantaneous response of the solid Earth to ice thickness changes over the small spatial aperture of the surge region was primarily elastic [*Sauber et al.*, 1995]. To represent some of the spatial complexity of a variable surface load, we chose to represent the change in glacial load by multiple disk loads each having a 5-km diameter. To approximate an equivalent rectangular load, the disks were multiplied by a geometrical scaling factor. The total displacement, **u**, **v**, at an individual geodetic station is the sum of the contributions from n disk loads L_i, $\sum_{i=1}^{n} u_i, \sum_{i=1}^{n} v_i$. The vertical displacement of the solid Earth, **u**, is useful for estimating the magnitude (and sign) of ice thickness changes. The horizontal component is particularly sensitive to the location (direction) of load changes.

5.4. Comparison of Observed and Predicted Displacements

Alternative models were tested against the 1993-1995 GPS displacement values by scaling the initial distribution of ice thickness change values above. We most closely matched the GPS results and remained consistent with the observed trimlines, with a scaling factor of 1.4. A set of unloading/loading disks that can account for the estimated station displacements is given in Plate 1 and the predicted horizontal and vertical displacements are shown in Plate 1 and Figure 2. The maximum thinning is estimated to be about 63 m, and the maximum ice thickening is 70 m. The predicted vertical depression ranges up to 102 mm in the region of increased ice thickness in the terminus region and the predicted uplift ranges up to 94 mm in the unloading region where the Bagley Ice Field flows into the Bering Glacier.

In Table 2 we compared the displacements predicted by our best fitting forward model to the geodetic observations. The observed displacement has had the estimated tectonic displacement removed [see *Sauber et al.*, 1997]. Of the sites used in this surge study, just DON had a third set of observations which enabled us to independently estimate the tectonic component of the displacement based on the 1995-1997 results. For ANCX, ISLE, and TIME the tectonic deformation rate had to be estimated on the basis of tectonic modeling of geodetic results from stations farther ($\geq$30 km) from the surge, and some additional uncertainty ($\pm$5 mm/yr) should be attributed to this approximation.

At the three sites nearest the surge (DON, ANCX, and ISLE) our model predictions minus the observed

(corrected) vertical displacement over the 1993-1995 time interval are less than the formal GPS uncertainty in the measured values (≈10 mm). The horizontal component is very sensitive to the direction of the ice mass change (i.e., changes in azimuth to unloading/loading will result in significant changes in magnitude and sign of the displacement). Because of limited glaciological and geodetic observations, we could use only a moderate resolution grid; this made it difficult to model the horizontal geodetic data in particular. We do not understand the large discrepancy between the observed and predicted north value for the station DON; the geodetic results seem to imply an ice mass change south of the stations.

The glaciological data (aerial photographs, field studies, and interferometric SAR study of ice velocities) were the primary constraints on the redistribution of ice mass, and we are confident of the general region that underwent thinning and thickening. The GPS data provided the most useful information near the stations ISLE and ANCX; here the ice thickness change uncertainty may be ±10-20 m (see the sensitivity analysis summarized by *Sauber et al.* [1997]). In other areas the uncertainties are larger and the magnitude and distribution of change were estimated primarily by glaciological studies.

5.5. Postsurge Changes to Bering Glacier and Bagley Ice Field

Between the cessation of the surge in 1995 and August 1999, the region that thickened and advanced during the surge has undergone thinning, and the terminus has retreated 0.1 to 1 km per year. The Bering Glacier piedmont lobe has a smooth surface once again. During the postsurge time period, most of the area below the ELA has experienced significant thinning. Although the surge initiation region may begin to build up ice thickness in the future owing to transfer of material from upglacier, it is not evident at this point.

6. Crustal Deformation Due to Glacial Recession This Century

Nearly all of the glaciers shown in Figure 1 have receded during this century [e.g., *Meier*, 1984], and many of these glaciers are still undergoing retreat. To calculate the predicted crustal deformation over the time span of our geodetic observations, we needed to estimate the Earth response to recent changes as well as the cumulative retreat over the last 100 years.

Here we report the available constraints on glacial retreat in the last 100 years. We calculated the surface deformation rate across the region due to an average annual ice thinning rate assuming a simple layered elastic Earth model. A two-dimensional finite element model was used to calculate the predicted displacement rate due to retreat. Because of our uncertain knowledge of the Earth's response on the time scale of tens of years, we explored simple variations in Earth rheology (i.e., especially the asthenospheric viscosity) assuming a theoretical retreat profile.

6.1. Glaciological Constraints

Some of the data we used for a rough characterization of ice thickness changes are given in Table 3; they include the elevation of moraine crests and trimlines in comparison to recent glacier surfaces. The Icy Bay glaciers have retreated ≈35 km from their turn of the century terminal position at the mouth of Icy Bay [*Plafker and Miller*, 1958; *Molnia*, 1977; *Porter*, 1989], and radiocarbon dating of lateral moraines suggest thinning of ≈300 m over this same time period (G. Plafker, field observations, 1963, 1969, 1982). The position of the Malaspina Glacier terminus is essentially stagnant. On the basis of trimline heights in the Samovar Hills and Chaix Hills, however, ≈140–180 m of thinning of the inner margin of the large piedmont lobe has occurred, probably during this century (G. Plafker, field observations, 1963, 1969, 1982; B. Molnia, field observations, 1974, 1989-1991, 1998). Thinning of the Bagley Ice Field and Tana Glacier during this century, but prior to the 1993–1995 surge, has been estimated to be 27 to 90 m at an average elevation of ≈1500 m [*Miller*, 1957; B. Molnia, field observations, 1974–1993; J. Sauber, field observations, 1993]. Between the 1967 surge and the onset of the most recent surge in 1993, the Bering Glacier terminus receded as much as 10 km and thinned as much as ≈180 m [*Molnia*, 1993; *Molnia and Post*, 1995]. The elevation changes along the centerline of Bering Glacier have been determined directly from a comparison of the 1972 and 1990–1992 elevations (Figure 1b of *Molnia and Post* [1995]). For the other glaciers in this region this level of detail is not available.

Where we do not have a direct estimate of ice thinning, we used the change in the position of the glacier terminus to determine a rough value. On the basis of a study of 15 mountain valley glaciers, the ratio of the thickness change averaged over the full length to the change in terminus position has been characterized by a profile shape factor, f, estimated at 0.1–0.4, with

an average value of ≈0.3 [*Schwitter and Raymond*, 1993]. It should be noted, however, that *Sapiano et al.* [1998] examined the elevation, volume, and terminus changes of nine glaciers in Alaska and Washington and found no simple relationship between volume change and terminus retreat. However, they found the elevation changes in most cases were largest near the terminus and decreased upglacier more rapidly than a linear variation with distance.

Field [1975] estimated the transition between the ablation and accumulation zone from the annual firn limit, a proxy for the ELA. He found that the average was generally around 1000 m (3280 feet) near the coast and the limit rises to about 1500 m (4920 feet) inland. We did not place disks representing unloading above these elevations.

6.2. Elastic Response to Average Yearly Thinning Rates

As was discussed in the preceding section, to represent some of the spatial complexity of a variable surface load, we chose to represent the change in glacial load by multiple disk loads. Since detailed information on retreat was not available for many parts of this region, we used a disk diameter of 10 km to represent average changes at this spatial scale (Figure 3), and we used *Farrell* [1972] to calculate the elastic displacement assuming a spherical Earth model. Also, we had to assume a temporal average over the time period of the constraints given in Table 3.

The calculated elastic uplift rate caused by the average yearly load reductions are given in Figure 3 for the horizontal component and in Figure 4 for the vertical component. The distributed elastic response to changing ice loads is up to 12 mm/yr of uplift and 2 mm/yr for the horizontal components.

We note that the differences between the horizontal (north and east) and vertical velocities of the five coastal stations (VYAK, FURR, YAKU, AMBR, and DON (1995-1997)) and the weighted mean of the individual components for all sites are less than 2σ except for the north and vertical component at the station AMBR (near Icy Bay). The uplift of AMBR (Icy Bay region) relative to VYAK (Yakataga region) is about 12 mm/yr (see Table 1), and the horizontal displacement rate relative to Yakataga is 6 mm/yr (mostly south). As can be seen in Figures 3 and 4, the predicted annual displacement due to retreat near the station AMBR is vertical uplift (about 3 mm/yr) and southward displacement (about 1 mm/yr).

As is evident in Figure 3 the orientation and magnitude of surface displacement rate are complex on the local and regional spatial scale. This illustrates the importance of good regional glaciological data to model displacement rates obtained from geodetic and tide gauge measurements. These calculations do not account for the viscoelastic response of the Earth to glacial unloading since early this century.

6.3. Viscoelastic Displacement Associated With Retreat

We used a two-dimensional plane strain finite element method (TECTON [*Melosh and Raefsky*, 1981]) to calculate the viscoelastic response of the Earth to glacier retreat during the past 100 years. The finite element grid across this subduction zone plate boundary is modified from *Cohen* [1996] and includes a shallow dipping subducting slab and both an oceanic crust-mantle and a continental crust-mantle (Figure 5). Since the details of crustal and upper mantle lithology and temperature gradient are not available across the study region, we relied on an estimate of the transitional depth from the epicenters of large earthquakes and the depth of background seismicity [e.g., *Scholz*, 1990]. In south central Alaska, upper plate background seismicity extends to less than 40 km [*Page et al.*, 1991], and the downgoing Pacific plate begins to bend at ≈22 km [*Plafker et al.*, 1994]. For the oceanic plate we assumed a transitional depth of around 30 km [*Sauber et al.*, 1993].

We used viscosities of 10^{25} Pa s for the upper crust (0-38 km) and 10^{21} Pa s for the upper mantle between 210 and 500 km. Owing to the uncertainty in the viscosity of the lower crust and upper mantle ($\geq$38 km to 210 km in our nonunique model for the continental plate and between 30 and 210 km below the oceanic plate), we calculated the predicted displacements by assuming a range of viscosities (5 x 10^{18} Pa s to 5 x 10^{21} Pa s). This range of numerical values is representative of those found from studies of postseismic and glacial rebound at the subduction boundary in Alaska [*Savage and Plafker*, 1991; *Cohen*, 1996; *Zheng et al.*, 1996] and Cascadia [e.g., *Wang et al.*, 1994; *James et al.*, 2000] and from lake unloading studies in a tectonically active region [e.g., *Bills et al.*, 1994]. This does not include a short-term, downdip low-viscosity zone or a creep zone used to account for rapid postseismic slip [e.g., *Wahr and Wyss*, 1980; *Cohen*, 1996].

The uplift rate due to glacial retreat during this century will be largest in the ablation zones of glaciers near the Gulf of Alaska coast. As is seen in Figure 1,

there is variation in the location of the glaciers relative to the coast. The Bering Glacier piedmont lobe has undergone advance during periodic surges followed by slow retreat of the ice front between surges, and the changes in the Bering Glacier lobe may have a small viscoelastic response. On the other hand, between the Malaspina Glacier and the glaciers to the west of Icy Bay, significant retreat and ice thinning (tens to hundreds of meters) have occurred, and we would expect a higher rebound in this area then, for example, near Cape Yakataga (Figure 1). Thus there is a suggestion that near Icy Bay the crustal deformation in response to the retreating glaciers may have a discernible influence on incremental tectonic strain data.

A general idealized longitudinal unloading profile for a retreating valley glacier is given in Figure 6 (after Figure 1 of *Schwitter and Raymond* [1993]). This roughly corresponds to a north-south profile that includes the site AMBR (Figure 3) and is near a site with carbon14 dating of an overridden forest. The estimated ice thickness change near this site is about 300 m (Table 3, site 1). For the region including the peak in Figure 6, spanned by a 10-km element in the finite element grid, a maximum of 300 m of ice thinning was assumed; the other elements were scaled on basis of the general profile from *Schwitter and Raymond* [1993]. For simplicity, we assumed that most glacier retreat and thinning occurred 100 years ago. We then calculated the predicted horizontal and vertical displacement predicted for shortly after the retreat until 100 years later.

For illustrative purposes, in Figure 7 we show the range of predicted deformation rates for 1, 50, and 100 years for the asthenospheric values given in Figure 5. The maximum uplift of about 3 m is centered near the Gulf of Alaska coast and drops to zero at $\approx$200 km inland from the coast; there is some migration of the maximum uplift away from the coast with time. Note that the station AMBR is located near the region of maximum rebound. In addition to the uncertainity associated with the GPS measurement results, the position of this site with respect to the actual ice thinning profile is approximate.

The range of deformation rates due to the viscoelastic response to retreat are compared in Table 4 with the uplift and horizontal rate of AMBR relative to VYAK. For asthenospheric viscosities $\geq 5 \times 10^{20}$ Pa s, very little time-dependent deformation over the 10 years that span our geodetic observations at the station AMBR is predicted. In contrast, with an asthenospheric viscosity of 5×10^{18} Pa s the vertical uplift rate due to the viscoelastic response was estimated to be about 31 mm/yr. A value of 5×10^{19} Pa s is most consistent with the observed rate, but the results from AMBR are not well determined, and our model contains simplifying assumptions. An uplift rate of ≥ 1 cm/yr probably cannot be accounted for by the annual expected thinning alone. An asthenospheric viscosity of less than 10^{20} Pa s may be necessary to account for the preliminary GPS results.

6.4. Crustal Deformation From Late Pleistocene Deglaciation

The last major Pleistocene deglaciation episode in Alaska is correlated with late Wisconsin fluctuations of the Laurentide Ice Sheet. Radiocarbon ages the show onset of glaciation at $\approx$24,000 B.P. and deglaciation beginning at about 13,500 B.P. [*Molnia*, 1989; *Hamilton*, 1994]. The late Pleistocene ice unloading model ICE-4G includes a simple representation of deglaciation in southern Alaska and was used to obtain a rough estimate of the solid Earth displacement caused by viscous relaxation [*Peltier*, 1993, 1994; T. James, personal communication, 1998]. An estimate of the present-day uplift attributable to this deglaciation was obtained by examining vertical displacements since 1000 B.P. obtained from files of topography change computed by W. R. Peltier. These files are available through the National Geophysical Data Center, Boulder, Colorado (see also the discussion by *James and Ivins* [1998]). Along a profile perpendicular to the coast near Cape Yakataga (Figure 1), the uplift rate caused by late Pleistocene deglaciation was estimated to be 2 mm/yr.

The asthenospheric viscosity of less than 10^{20} Pa s suggested for our study region is lower than that derived for global postglacial rebound associated with continental scale glacial retreat in the late Pleistocene [e.g., *Peltier*, 1994]. It should be noted that the uplift data used in the later study were primarily from nontectonic regions, and much of the late Pleistocene deglaciation occurred at interior plate regions. The ICE-4G results thus give an upper bound on the uplift rate in southern Alaska due to late Pleistocene deglaciation. With a lower asthenospheric viscosity the predicted uplift due to late Pleistocene deglaciation would be even smaller, since most of the rebound would have occurred much earlier.

6.5. Coastal Uplift Rates Between Icy Bay and Bering Glacier

Table 1 presents estimates of the horizontal and vertical rates of deformation from GPS observations made between 1993 and 1997, and Table 5 gives the uplift rates estimated from carbon14 dating of terraces uplifted over the last 3000-6000 years. Since this is a region of large earthquakes, significant elastic strain is accumulating which will eventually be released in earthquakes, and the short-term strain is thought to be primarily elastic. These earthquakes could cause slip on the plate interface and/or on faults within the overriding plate, causing crustal shortening and permanent uplift. Coseismic slip on faults within the overriding plate is suggested by $\approx$1 m of probable coseismic uplift between Icy Bay and Yakataga during the great 1899 Yakutat Bay earthquake sequence [*Tarr and Martin*, 1912; *Thatcher and Plafker*, 1977, unpublished manuscript, 1977]. Estimates of the uplift rate over the last $\approx$6000 years suggest 7–15 mm/yr of uplift near Icy Bay but only 2–3 mm/yr near the Bering Glacier (Table 3, *Plafker et al.* [1981] and *Molnia and Post* [1995]). Thus more onshore crustal shortening may occur in the Icy Bay region. Also, as was discussed above, it may be that in the recently deglaciated region of Icy Bay there may be some additional short-term uplift due to rebound.

7. Glacial Fluctuations and Earthquakes

The ice mass changes due to the glacial fluctuations discussed above perturb the local and regional stress field. The spatial (Plate 1) and temporal (1-2 years) scales, as well as the magnitude, of loading and unloading associated with the Bering Glacier surge is similar to water reservoir impoundment or the removal of rock in a quarry. For this case, the finite strength of the lithosphere will support the load, and the elastic, deviatoric stresses will decrease as a function of depth [e.g., *Scholz*, 1990; *Cohen*, 1993]. The retreat of the coastal Alaska glaciers during this century has occurred over a broader spatial scale, and some flow in the asthenosphere is assumed to have occurred. Eventually, this flow will bring the Earth back into isostatic equilibrium. In the glacial retreat case, there will be time-dependent changes in surface and subsurface stress distribution even if the load does not continue to change.

We evaluated the possible influence of glacial fluctuations on earthquake occurrence and surface faulting by presenting the predicted stress changes in the context of a simple Navier-Coulomb failure criterion. For the surge case we tested if there was a concurrent seismicity change in the area of the surge reservoir region where ice thinning occurred and/or in the surge receiving area where ice thickening and advance occurred. Since retreat of the coastal Alaska glacier started approximately 100 years ago, we can not easily test for temporal variations in earthquake occurrence. We compared the seismicity in recently deglaciated regions to regions at greater distance from retreating glaciers.

7.1. Magnitude and Orientation of Principal Stresses

Earthquake focal mechanisms, offshore in situ borehole measurements, the geodetic estimate of incremental strain, and regional geological evidence [*Estabrook and Jacob*, 1991; *Plafker et al.*, 1994; *Doser et al.*, 1997; *Sauber et al.*, 1997] have been used to estimate principal shortening and stress directions. For the coastal region between Icy Bay and Kayak Island, a horizontal north-south to northwest-southeast orientation is suggested for the maximum effective stress (σ_1), and a minimum effective stress (σ_3) that is vertical has been assumed for the dominantly thrust faulting environment (Figure 1). Strike-slip faulting associated with vertical intermediate stress (σ_2) conditions has been suggested near the Contact fault just north of the Bagley Ice Field [*Savage and Lisowski*, 1988].

Borehole failure observed in offshore wells between Icy Bay and Kayak Island have been reported by *Hottman et al.* [1979]. In general, breakouts have their long axis parallel to the minimum horizontal stress so that they can be used to map horizontal principal stress trajectories and identify the relative horizontal stress magnitudes [*Adams and Bell*, 1991]. On the basis of the prevalence of thrust faulting in the area and independent information on the orientation of the maximum horizontal stress direction, *Hottman et al.* [1979] estimated the orientation and the approximate magnitudes of principal stresses. In their calculations it was assumed that the three principal Earth stresses were oriented almost vertically and horizontally. The overburden stress, taken to be σ_v, was estimated from well interval density logs. They calculated Earth stress gradients of σ_1 = 32 kPa/m, σ_2 = 27 kPa/m, and $\sigma_v = \sigma_3$ = 23 kPa/m, and pore pressure p_o = 19.2 kPa/m from cores cut between 2700 and 4000 m. In Figure 8, the estimated effective

stress for σ_1 and σ_3 were extrapolated to a depth of 5 km.

7.2. Shear Failure

The Mohr-Coulomb criterion for brittle shear failure in rock is described by

$$\tau = \tau_o + \mu\sigma_n, \quad (1)$$

where τ is the shear stress necessary to induce failure on a fault plane, τ_o is the inherent shear strength of the fault, μ is the coefficient of friction of the fault surface, and σ_n is the normal stress on the fault [*Jaeger*, 1969]. The locus of shear (τ) and normal (σ_n) stress components on a suite of faults of various orientations is a Mohr circle whose center is the average between the maximum (σ_1) and minimum (σ_3) principal stresses and whose radius is $(\sigma_1 - \sigma_3)/2$.

Laboratory studies indicate for intact rock samples that $\tau_o \approx 50$ MPa and $\mu = 0.6$ to 0.85 (e.g., see the summary by *Johnston* [1987]). For a region such as southern Alaska that is heavily faulted, we assume that faults with fault gouge exist at a variety of orientations. Additionally, when preexisting faults with fault gouge are present, μ may be as low as 0.2–0.4, τ_o approaches zero, and equation (1) becomes

$$\tau = (0.4 - 0.85)\sigma_n. \quad (2)$$

For faults with low friction, in fact, slip on faults over a range of orientations would occur.

7.3. Stress Drop in Recent Earthquakes

A number of large earthquakes have occurred in the last 30 years within or near the study region given in Figure 1 (1987–1988, Gulf of Alaska, $M_S = 6.9$, 7.6, 7.6; 1979, St. Elias, $M_S = 7.2$; 1970, Pamplona zone $M_W = 6.7$). The static stress drop in the St. Elias and Gulf of Alaska earthquakes ranges from moderate to high ($\approx$2 to 10 MPa) [*Hwang and Kanamori*, 1992; *Estabrook et al.*, 1992; *Sauber et al.*, 1993; *Doser et al.*, 1997]. Although stress levels on individual faults are highly variable, these earthquakes suggest that much of the region given in Figure 1 is close to failure. The last $M_S \geq 8.0$ earthquakes occurred in 1899. In Figure 8 we present the stress drop in these earthquakes relative to other stress changes.

7.4. Surge Case

Water loading, quarry unloading, and changes in glacier mass cause a static change in load and pore pressure equivalent to the water or rock thickness (see the summary by *Scholz* [1990]). A comparison of well-documented case histories of seismicity near water reservoirs suggests that primarily two types of induced seismicity are observed (see the summary by *Simpson et al.* [1988]). Changes in seismicity which follow rapidly after the filling of a reservoir are related to changes in elastic stress or changes in pore pressure coupled to the elastic stress. Since the stress increase from the elastic load drops off rapidly with distance, seismicity in these cases is concentrated in the immediate vicinity of the reservoir, and earthquake sizes tend to be small, since the stress gradients are high. *Simpson et al.* [1988] further observed that where there is a long delay between the filling of the reservoir and the start of increased seismicity, diffusion of pore pressure from the reservoir to hypocentral depths may play a dominant role.

In the dominantly thrust earthquake environment of the study region, the direct effect of ice loading in the surge receiving region will be to increase σ_3, which reduces the likelihood of earthquake faulting, whereas for the unloading region it will decrease σ_3 and make failure more likely. At shallow crustal depths the immediate poroelastic effect could also be important. However, after the cessation of the surge, the Bering Glacier started to retreat once again; so we did not evaluate the possibility of later triggering due to pore pressure diffusion.

We examined the background seismicity ($M_L \geq 2.5$) before (1991.0–1993.4), during (1993.4–1995.8), and after (1995.8–1998.3) the Bering Glacier surge to see if a short-term change in either the rate or location of small to moderate earthquakes occurred. Although the general regional level of seismicity varies only slightly over the three time periods, there is an increased level of seismicity under the region of greatest thinning during the surge (Figure 9). An ice thickness change of 50 m corresponds to a change in the σ_3 (vertical) of approximately 0.5 MPa. This is consistent with the idea that σ_3 (vertical) is decreased (Figure 8) and failure in thrust type earthquakes would be more likely; the focal mechanism solutions, however, for these small earthquakes are unknown.

7.5. Retreat Case

We used the plane strain viscoelastic calculations described in an earlier section to examine the estimated stress changes as a function of time and depth. The calculated values represent average values over the elements given in Figure 5. For our reference

model (Figure 5) the maximum decrease in σ_V between 0 and 10 km was $\approx$1.0 MPa. This stress change is significant in relation to the stress drops in recent earthquakes ($\approx$2 to 10 MPa) but small in relation to the estimated stress magnitude. Therefore the occurrence of an earthquake may be advanced, but the ongoing stress accumulation would be primarily due to tectonic forces. This is consistent with the results of numerical simulations of a fault surface with tectonic loading by *Rydelek and Sacks* [1999] which suggest that incremental stress changes of several tenths of a bar (0.1 MPa) significantly affects the time of an earthquake but not its size or its location.

The location of $M_L \geq 4.0$ earthquakes between 1973 and 1997 was examined to see if there was a spatial concentration near regions of glacial retreat. In 1979 a large earthquake (St. Elias, $M_S = 7.2$) occurred inland from Icy Bay, and the aftershocks associated with this event are evident in Figure 10. The source mechanism for this event indicates underthrusting on a northeast dipping plane with a source depth of 24 km [*Estabrook et al.*, 1992]. It is possible that the occurrence of this earthquake was advanced due to a decrease in σ_v due to glacial retreat.

The orientation of postglacial stress release features such as pop-ups and faulting in regions that underwent extensive late Pleistocene deglaciation suggest that they were caused by near-surface stresses dominanted by radial flexural (fiber or longitudinal) stresses near the retreating ice margin [*Adams*, 1989; *Adams and Bell*, 1991]. Determination of focal mechanisms for shallow earthquakes occurring below recently deglaciated coastal regions could test this hypothesis.

7.6. Loading Associated With Offshore Sedimentation

The high uplift rates within the ablation zone of the coastal glaciers has led to high erosional rates. This then leads to high sedimentation rates in offshore basins [*Molnia*, 1989; *Eyles et al.*, 1991]. *Bird* [1996] speculated that the present localization of crustal shortening is a transient effect of Pliocene-Pleistocene glaciations which have removed mass from the coastal mountains and redistributed it onto the eastern forearc. He postulated that this may have upset the balance between forearc slope and basal traction on the plate interface, requiring the onshore part of the forearc to be shortened and uplifted to restore the dynamic equilibrium.

Sediment loading would increase σ_v and, in a thrust earthquake environment, inhibit earthquakes. The average thickness of Holocene sediments on the south central Alaska continental shelf is about 45 m with a maximum thickness of 350 m south of Copper River (west of our study region) [*Molnia et al.*, 1980]. On the basis of vertical stress and pore pressures estimated from the borehole data summarized above, this additional loading corresponds to an effective σ_v that ranges from less than 1 MPa to 1.3 MPa. Since the end of the Little Ice Age, sedimentation rates near Icy Bay have been measured to be more than 1 m/yr [*Molnia*, 1979]. This corresponds to an effective σ_v of almost 1 MPa. Once again these stresses are significant, but we suggest that this would only perturb the dominant tectonic stress field.

8. Summary

In this study we have estimated crustal deformation rates and stress changes in response to ice mass changes associated with two major glacial fluctuations in the coastal region of southern Alaska between the Malaspina and Bering Glaciers. Large uplift and subsidence on a local scale occurred in response to the ice mass redistribution during the Bering Glacier surge. An increase in the occurrence of small earthquakes beneath the surge reservoir region may be due to a decrease in the vertical load in this thrust earthquake environment. Glaciological constraints supplemented by our geodetic results were used to estimate the ice mass redistribution during the surge. Our results suggest that geodetic data provide new information and constraints on ice lowering in the surge reservoir region where there is less glaciological information.

Surface displacements due to the Earth's viscoelastic response to retreat of the coastal glaciers during this century were also calculated. The predicted yearly uplift rates associated with the rebound processes are generally small. However, in the ablation zone near Icy Bay the preliminary vertical uplift rate, relative to Cape Yakataga, was large enough to be measured geodetically, and it may place bounds on upper mantle viscosities. The cumulative stress changes in the deglaciated region are significant in relation to the stress drop in earthquakes but small in relation to the estimated tectonic stress levels. Ice mass removal could trigger earthquakes earlier than would otherwise have been the case, but the primary source of stress accumulation is due to ongoing tectonic processes.

Acknowledgments. We thank Bob King, Simon McClusky, Tom Herring, and Danan Dong for GAMIT and GLOBK help; Michael Lisowski and James Savage for logistical background on the Yakataga area; Steve Cohen for discussions on the finite element modeling and review of the manuscript; and Rob Fatland for helpful discussions on the Bering Glacier surge. The careful reviews of Thomas James, Craig Lingle, and the JGR associate editor, Robert King, were greatly appreciated. The GPS observations in the Yakataga region were made with the invaluable field assistance of Garth Franklin at JPL and Bjorn Johns at UNAVCO. Copies of ERS1 data from the Bering Glacier Project were obtained from Robb Macleod at Ducks Unlimited and John Payne of BLM. This research was supported by grants from NASA's Solid Earth and Natural Hazards program to J. Sauber.

References

Adams, J., Postglacial faulting in eastern Canada: Nature, origin and seismic hazard implications, *Tectonophysics, 163,* 323–331, 1989.

Adams, J., and J. S. Bell, Crustal stresses in Canada, in *Neotectonics of North America, Decade of N. Am. Map,* vol. 1, edited by D. B. Slemmons, E. R. Engdahl, M. D. Zoback, and D. D. Blackwell, Geol. Soc. of Am., Boulder, Colo., 1991.

Bard, E., H. Bruno, and R. G. Fairbanks, U-Th ages obtained by mass spectrometry in corals from Barbados: Sea level during the past 130,000 years, *Nature, 346,* 456–458, 1990.

Bills, B. G., D. R. Currey, and G. A. Marshall, Viscosity estimates for the crust and upper mantle from patterns of lacustrine shoreline deformation in the Eastern Great Basin, *J. Geophys. Res., 99,* 22,059–22,086, 1994.

Bird, P., Computer simulations of Alaskan neotectonics, *Tectonics, 15,* 225–236, 1996.

Boucher, C., Z. Altamimi, M. Feissel, and P. Sillard, Results and analysis of the ITRF94, *IERS Tech. Note 20,* Central Bur. of the IERS, Obs. de Paris, Paris, 1996.

Budd, W. F., and B. J. McInnes, Modeling periodically surging glaciers, *Science, 186,* 925–927, 1974.

Clark, J. A., An inverse problem in glacial geology: The reconstruction of glacier thinning in Glacier Bay, Alaska between A.D. 1910 and 1960 from relative sea-level data, *J. Glaciol., 18,* 481–503, 1977.

Cohen, S. C., Does rapid change in ice loading modulate strain accumulation and release in glaciated, tectonically active regions?, *Geophys. Res. Lett., 20,* 2123–2126, 1993.

Cohen, S. C., Time-dependent uplift of the Kenai Peninsula and adjacent regions of south central Alaska since the 1964 Prince William Sound earthquake, *J. Geophys. Res., 101,* 8595–8604, 1996.

DeMets, C., R. G. Gordon, D. Argus, and S. Stein, Effect of recent revisions to the geomagnetic reversal time scale on estimates of current plate motions, *Geophys. Res. Lett., 21,* 2191–2194, 1994.

Dolgushin, L. D., and G. B. Osipova, Glacier surge and the problem of their forecasting, *Int. Assoc. of Sci. Hydrol., 104,* 292–304, 1975.

Doser, D. I., J. R. Pelton, and A. M. Veilleux, Earthquakes in the Pamplona zone, Yakutat block, south central Alaska, *J. Geophys. Res., 102,* 24,499–24,511, 1997.

Estabrook, C. H., and K. H. Jacob, Stress indicators in Alaska, in *Neotectonics of North America, Decade of N. Am. Map,* vol. 1, edited by D. B. Slemmons, E. R. Engdahl, M. D. Zoback, and D. D. Blackwell, pp. 387–399, Geol. Soc. of Am., Boulder, Colo. 1991.

Estabrook, C. H., J. L. Nabelek, A. L. Lerner-Lam, Tectonic model of the Pacific-North American plate boundary in the Gulf of Alaska from broadband analysis of the 1979 St. Elias, Alaska, earthquake and its aftershocks, *J. Geophys. Res., 97,* 6587–6612, 1992.

Eyles, C. H., N. Eyles, and M. B. Lago, The Yakataga formation: A late Miocene to Pleistocene record of temperate glacial marine sedimentation in the Gulf of Alaska, in *Glacial Marine Sedimentation: Paleoclimatic Significance,* edited by J. B. Anderson and G. M. Ashley, *Spec. Pap. Geol. Soc. of Am., 261,* 159–180, 1991.

Fang, P., and Y. Bock, Scripps Orbit and Permanent Array Center report, in *The IGS 1994 Annual Report, Int. GPS Serv. for Geodyn.*, edited by J. F. Zumberge, R. Liu, and R. E. Neilan, pp. 213–233, IGS Central Bur., Jet Propul. Lab., Pasadena, Calif., 1995.

Farrell, W. E., Deformation of the Earth by surface loads, *Rev. Geophys., 10,* 761–797, 1972.

Fatland, D. R., Studies of Bagley Ice Field during surge and Black Rapids Glacier, Alaska, using spaceborne SAR interferometry, Ph.D. Thesis, 97 pp., Univ. of Alas. Fairbanks, Dec., 1998.

Fatland, D. R., and C. S. Lingle, Analysis of the 1993-95 Bering Glacier surge using differential SAR interferometry, *J. Glaciol., 44,* 532–546, 1998.

Feigl, K. L., et. al., Space geodetic measurement of crustal deformation in central and southern California, 1984–1992, *J. Geophys. Res., 98,* 21,677–21,712, 1993.

Field, W. O., Glaciers of the St. Elias and Chugach Mountains, in *Mountain Glaciers of the Northern Hemisphere,* edited by W. O. Field, vol. 2, pp. 233–492, U.S. Army Corps of Eng., Hanover, N.H., 1975.

Hager, B. H., Weighing the ice sheets using space geodesy: a way to measure changes in ice sheet mass (abstract), *Eos Trans. AGU, 72*(17), Spring Meet. Suppl. 91, 1991.

Hager, B. H., R. W. King, and M. H. Murray, Measurement of crustal deformation using the Global Positioning System, *Annu. Rev. Earth Planet. Sci., 19,* 351–382, 1991.

Hamilton, T. D., Late Cenozoic glaciation of Alaska, in *The Geology of North America*, vol. G-1, *The Geology of Alaska*, edited by G. Plafker and H. C. Berg, pp. 813–844, Boulder, Colo., 1994.

Herring, T. A., GLOBK, Global Kalman filter VLBI and GPS analysis program version 4.1, Mass. Inst. of Technol., Cambridge, 1997.

Herzfeld, U. C., and H. Mayer, Surge of Bering Glacier and Bagley Ice Field, Alaska: an update to August 1995 and an interpretation of brittle deformation patterns, *J. Glaciol., 143,* 427–434, 1997.

Hottman, C. E., J. H. Smith, and W. R. Purcell, Relationship among Earth stresses, pore pressure, and drilling problems offshore Gulf of Alaska, *J. Pet. Technol.*, vol. 31, 1477–1484, 1979.

Hwang, L. J., and H. Kanamori, Rupture processes of the 1987-1988 Gulf of Alaska earthquake sequence, *J. Geophys. Res., 97,* 19,881–19,908, 1992.

Jaeger, J. C., *Elasticity, Fracture and Flow with Engineering and Geological Applications*, 268pp., Methuen, New York, 1969.

James, T. S., and E. R. Ivins, Present-day Antarctic ice mass changes and crustal motion, *Geophys. Res. Lett., 22,* 973–976, 1995.

James, T. S., and E. R. Ivins, Predictions of Antarctic crustal motions driven by present-day ice sheet evolution and by isostatic memory of the last glacial maximum, *J. Geophys. Res., 103,* 4993–5017, 1998.

James, T. S., J. J. Clague, K. Wang, and I. Hutchinson, Postglacial rebound at the northern Cascadia subduction zone, *Quaternary Science Reviews: Ice Sheets, Crustal Deformation and Seismicity*, eds. I. Stewart and J. Sauber, Elsevier, Amsterdam, in press, 2000.

Johnston, A. C., Suppression of earthquakes by large continental ice sheets, *Nature, 330,* 467–469, 1987.

Kamb, B., C. Raymond, W. Harrison, H. Engelhardt, K. Echelmeyer, N. Humphrey, M. Brugman, and T. Pfeffer, Glacier surge mechanism: 1982-1983 surge of Variegated Glacier, Alaska, *Science, 227,* 469–479, 1985.

Karato, S., and P. Wu, Rheology of the upper mantle: A synthesis, *Science, 260,* 771–778, 1993.

Kaufmann, G., and P. Wu, Lateral asthenospheric viscosity variations and postglacial rebound: a case study for the Barents Sea, *Geophys. Res. Lett., 25,* 1963–1966, 1998.

King, R. W., and Y. Bock, Documentation for the GAMIT GPS analysis software: GAMIT, version 9.6, Mass. Inst. of Technol., Cambridge, 1997.

Kirby, S. H., Rock mechanics observations pertinent to the rheology of the continental lithosphere and the localization of strain along shear zones, *Tectonophysics, 119,* 1–27, 1985.

Krimmel, R. M., Photogrammetric measurement of geometric changes of Bering Glacier during the 1993-94 surge (abstract), *Eos Trans. AGU, 75*(44), Fall Meet. Suppl., 62, 1994.

Lingle, C. S., A. Post, U. C. Herzfeld, B. F. Molnia, R. M. Krimmel, and J. J. Roush, Bering Glacier surge and iceberg-calving mechanism at Vitus Lake, Alaska, U.S.A., *J. Glaciol., 39,* 722–727, 1993.

Mao, A., C. G. A., Harrison, and T. H. Dixon, Noise in GPS coordinate time series, *J. Geophys. Res., 104,* 2797–2816, 1999.

Meier, M. F., Contribution of small glaciers to global sea level, *Science, 226,* 1418–1421, 1984.

Meier, M. F., and A. Post, What are glacier surges?, *Can. J. of Earth Sci., 6,* 807–817, 1969.

Melosh, H. J., and A. Raefsky, A simple and efficient method for introducing faults into finite element computations, *Bull. Seismol. Soc. Am., 71,* 1391–1400, 1981.

Miller, D. J., The surface velocity of the Yakataga Glacier, Alaska, *J. Glaciol., 3,* 125–130, 1957.

Molnia, B. F., Rapid shoreline erosion and retreat at Icy Bay, Alaska–A staging area for offshore petroleum development, *Proc. Offshore Technol. Conf., 8,* 115–126, 1977.

Molnia, B. F., Sedimentation in coastal embayments in the northern Gulf of Alaska, *Proc. Offshore Technology Conference, 1,* 665–676, 1979.

Molnia, B. F., Subarctic (temperate) glacial-marine sedimentation–The northeast Gulf of Alaska. in *Glacial-Marine Sedimentation, 28th International Geological Congress, Short Course, Geol. Ser.*, vol. 9, edited by J.B. Anderson and B.F. Molnia, pp. 59–106, AGU, Washington, D.C., 1989.

Molnia, B. F., Major surge of the Bering Glacier, *Eos Trans. AGU, 74,* 321–322, 1993.

Molnia, B. F., and A. Post, Holocene history of Bering Glacier, Alaska: A prelude to the 1993-1994 surge, *Phys. Geogr., 16,* 87–117, 1995.

Molnia, B. F., W. P. Levy, and P. R. Carlson, Map of Holocene sedimentation rates in the northeastern Gulf of Alaska, *U. S. Geol. Surv., Misc. Field Stud. Map, MF-1170,* 1980.

Molnia, B. F., A. Post, D. C. Trabant, and R. M. Krimmel, The 1993-94 surge of Bering Glacier, Alaska: An overview (abstract), *Eos Trans. AGU, 75*(44), Fall Meet. Suppl., 62, 1994.

Muller, E. H., and P. J. Fleisher, Surging history and potential for renewed retreat: Bering Glacier, Alaska, U.S.A., *Arct. Alp. Res., 27,* 81–88, 1995.

Page, R. A., N. N. Biswas, J. C. Lahr, and H. Pulpan, Seismicity of continental Alaska, in *Neotectonics of North America, Decade of N. Am. Map*, vol. 1, edited by D. B. Slemmons, E. R. Engdahl, M. D. Zoback, D. D. Blackwell, Geol. Soc. of Am., Boulder, Colo., 1991.

Peltier, W. R., Time dependent topography through glacial cycle, *IGBP PAGES/Cent.A for Paleoclimatol. Data Contrib. Ser. 93-015,* NOAA/NGDC Paleoclimatol. Program, Boulder, Colo., 1993.

Peltier, W. R., Ice age paleotopography, *Science, 265,* 195–201, 1994.

Peltier, W. R., and J. T. Andrews, Glacial isostatic adjustment, I, The forward problem, *Geophys. J. R. Astron. Soc., 46,* 605–646, 1976.

Plafker, G., and D. J. Miller, Glacial features and surficial deposits of the Malaspina district, Alaska, *U.S. Geol. Surv. Misc. Geol. Invest. Map, I-271,* 1958.

Plafker, G., T. Hudson, M. Rubin, and K. L. Dixon, Holocene marine terraces and uplift history in the Yakataga seismic gap near Icy Cape, Alaska, *U.S. Geol. Surv. Circ., 844,* 111–115, 1981.

Plafker, G., L. M. Gilpin, and J. C. Lahr, Neotectonic map of Alaska, scale 1:2,500,000, in *Geology of Alaska, Map, GNA–G–1,* , Plate 12a, Geol. Soc. of Am., Boulder, Colo., 1994.

Porter, S. C., Late Holocene fluctuations of the fiord glacier system in Icy Bay, Alaska, U.S.A., *Arct. and Alp. Res., 21,* 364–379, 1989.

Roush, J.J., The 1993–1994 surge of Bering Glacier, Alaska observed with satellite synthetic aperture radar, M.S. thesis, Univ. of Alas., Fairbanks, 1996.

Rydelek, P. A., and I. S. Sacks, Large earthquake occurrence affected by small stress changes, *Bull. Seismol. Soc. Am., 89,* 822–828, 1999.

Sapiano, J. J., W. D. Harrison, and K. A. Echelmeyer, Elevation, volume, and terminus changes of nine glaciers in North America, *J. Glaciol., 44,* 119–135, 1998.

Sauber, J., T. A. Clark, L. J. Bell, M. Lisowski, C. Ma, and D. S. Caprette, Geodetic measurement of static displacement associated with the 1987-1988 Gulf of Alaska earthquakes, in *Contributions of Space Geodesy to Geodynamics: Crustal Dynamics, Geodynamics 23,* 233–248, 1993.

Sauber, J., G. Plafker, and J. Gipson, Geodetic measurements used to estimate ice transfer during Bering Glacier surge, *Eos Trans. AGU, 76,* 289–290, 1995.

Sauber, J., S. McClusky, and R. King, Relation of ongoing deformation rates to the subduction zone process in southern Alaska, *Geophys. Res. Lett., 24,* 2853–2856, 1997.

Savage, J. C., and M. Lisowski, Deformation in the Yakataga seismic gap, southern Alaska, 1980–1986, *J. Geophys. Res., 93,* 4731–4744, 1988.

Savage, J. C., and G. Plafker, Tide gauge measurements of uplift along the south coast of Alaska, *J. Geophys. Res., 96,* 4325–4335, 1991.

Scholz, C. H., *The Mechanics of Earthquakes and Faulting,* pp. 324–333, Cambridge Univ. Press, New York, 1990.

Schwitter, M. P., and C. F. Raymond, Changes in the longitudinal profiles of glaciers during advance and retreat, *J. Glaciol., 39,* 582–590, 1993.

Simpson, D. W., W. S. Leith, and C. H. Scholz, Two types of reservoir induced seismicity, *Bull. Seismol. Soc. Am., 78,* 2025–2040, 1988.

Stuiver, M., and P. J. Reimer, Extended ^{14}C data base and revised calib. 3.0 ^{14}C age calibration program, *Radiocarbon, 35,* 215–230, 1993.

Tarr, R. S., and L. Martin, The earthquakes of Yakutat Bay, Alaska, *U.S. Geol. Surv., Prof. Pap. 69,* 135 pp., 1912.

Thatcher, W., and G. Plafker, The 1899 Yakutat Bay, Alaska earthquakes, paper presented at IASPEI/IAVCEI Assembly, Int. Union of Geod. and Geophys., Durham, England, 1977.

Wahr, J., and W. Wyss, Interpretation of postseismic deformation with a viscoelastic relaxation model, *J. Geophys. Res., 85,* 6471–6477, 1980.

Wahr, J., D. Han, and A. Trupin, Predictions of vertical uplift caused by changing polar ice volumes on a viscoelastic Earth, *Geophys. Res. Lett., 22,* 977–980, 1995.

Wang, K., H. Dragert, and H. J. Melosh, Finite element study of uplift and strain across Vancouver Island, *Can. J. Earth Sci., 31,* 1510–1522, 1994.

Zheng, G., R. Dmowska, and J. R. Rice, Modeling earthquake cycles in the Shumagin subduction segment, Alaska, with seismic and geodetic constraints, *J. Geophys. Res., 101,* 8383–8392, 1996.

M. Bryant, ASHTECH, 12030 Sunrise Valley Drive, Reston, VA, 20191

B. Molnia, MS 917, U.S. Geological Survey, Reston, VA 20192

G. Plafker, MS 904, U.S. Geological Survey, Menlo Park, CA 94025

J. Sauber, Code 921, NASA's Goddard Space Flight Center, Greenbelt, MD 20771. (e-mail: jeanne@steller.gsfc.nasa.gov)

Received November 17, 1998; revised December 3, 1999; accepted December 3, 1999.

[1]Geodynamics Branch, NASA's Goddard Space Flight Center, Greenbelt, Maryland

[2]U.S. Geological Survey, Menlo Park, California

[3]U.S. Geological Survey, Reston, Virginia

[4]ASHTECH, Reston, Virginia.

This preprint was prepared with AGU's LaTeX macros v5.01. File bgreprint formatted January 27, 2000.

Figure 1. Glaciers of the eastern Chugach Mountains, Bering Glacier area, and the western portion of the glaciers of the St. Elias Mountains, Yakutat Bay area (modified from *Field* [1975]). The triangles indicate the location of GPS sites (see Table 1). The numbered dots correspond to sites where the ice thinning estimates listed in Table 3 were made. The Bagley Ice Field occupies a long, narrow east-west trending basin and flows primarily westward to the Bering Glacier. Southeast of the Bagley Ice Field is the neve whose principal outlets are the Yahtse and Guyot Glaciers in Icy Bay. Farther to the east, a neve in the St. Elias Range is the source region for the Malaspina Glacier. The inset shows the region covered by Figure 1.

Figure 2. A contour plot of the predicted uplift and subsidence (millimeters) of the solid Earth associated with the loading/unloading shown in Plate 1. Comparisons of the observed versus predicted displacements are given in Table 2. The base map of Plate 1 was used.

Figure 3. Predicted horizontal elastic displacement rate of the solid Earth associated with recent retreat of the coastal glaciers. Disks used to represent the annual unloading rate over the last 30–100 years (circles); the magnitude of unloading in meters per year is given from top left to bottom right: -1, -1, -1, -1, -1, -1, -1, -1, -1, -1, -2, -2, -2, -2, -1, -4, -6, -6, -4, -2, -6, -6, -1 -2, -1, -2, -1, -2, -2, -2, -4, -4, -3, -2, -1.5, -1, -1, -1, -1, -1, -1.5, -1.5, -1.5, -1.5, -1, -1, -1.5, -1.5, -1.5, -1.5, -1, -1, -1, -1. The primary sites occupied with GPS are given by triangles. The Gulf of Alaska coastline is shown by a thick solid line and a simplified outline of the glaciers is given by a thinner solid line.

Figure 4. Contour plot of the predicted elastic uplift and subsidence rate (millimeters per year) of the solid Earth associated with the unloading given in Figure 3.

Figure 5. Finite element grid represention of the subduction zone plate boundary used to calculate the viscoelastic response of the Earth to glacial unloading (modified from *Cohen* [1996]). Given within the key are the assumed elastic parameters (E) and viscosity (μ), in Pa s, for the reference model.

Figure 6. Schematic of the ice thickness change in the longitudinal profile of a retreating glacier used as input to the finite element calculation (after Figure 1 of *Schwitter and Raymond* [1993]). For the region including the peak spanned by a 10 km element in the finite element grid, a maximum value of 300 m was assumed; the other elements were scaled on the basis of the profile given.

Plate 1. Predicted horizontal elastic displacement field (millimeters) of the solid Earth associated with ice transfer during the Bering Glacier surge and some thinning due to retreat (black disks, in meters -21, -21) over the 1993-1995 time frame. The disks are used to represent unloading (red) and loading (blue) in meters (-14, -42, -63, -63, -42, -42, -21, -7, -7, -7, -49, -49, -14, -28, -21 -7, -21, -21, -14, -14, -7) and ice loading (14, 14, 14, 14, 14, 14, 14, 14, 14, 14, 42, 42, 63, 56, 70, 70, 70). The triangles indicate the three sites adjacent to the surge region (DON, ANCX, ISLE), one site within ≈20 km of the surge reservoir region (TIME), and a reference site (VYAK). A satellite synthetic aperture radar image of the Bering Glacier and the Bagley Ice Field was used as a base map (see Figure 1 from *Lingle et al.* [1993]). The thick solid line near DON and VYAK indicates the approximate position of the Gulf of Alaska coast, and the thin solid line indicates the edges of the Bering Glacier and Bagley Ice Field.

Plate 2. Oblique aerial photograph of the Jeffries Glacier (top) and Bagley Ice Field (bottom), a portion of the Bering Glacier, separated by Juniper Island, and a nunatak in the Chugach Mountains, Alaska. The trimline and thick lateral moraine draped around the exposed bedrock is indicative of the significant recent thinning that both glaciers have experienced. More than 50 m of post-1993 thinning of the Bering Glacier (foreground) has occurred. This is due to removal and downglacier transfer of ice during the 1993–1995 surge and postsurge ablation.

Figure 7. a. Predicted uplift after 1 year (solid line), after 50 years (dash-dot line), and over 100 years (dashed line) for the model parameters given in Figure 5. Here the distance from trench refers to the distance from the 2800-m contour near the Transition fault [*Plafker et al.*, 1994]. (b.) Predicted horizontal (north-south) displacement rate for times as in 7a. A positive displacement rate is toward the trench ($\approx$ south).

Figure 8. The Navier-Coulomb failure representation of the stress state of coastal Alaska between Icy Bay and Kayak Island. The failure envelope is given for $\tau = 0.4\sigma_n$ and $\tau = 0.85\sigma_n$. The Mohr circle representation of the effective stresses has been estimated for a depth of 5 km. The estimated stress drop for recent earthquakes is compared to the estimated stress with sediment loading over the last 10,000 years, ice mass redistribution during the Bering Glacier surge, and retreat this century.

Figure 9. Earthquakes of $M_L \geq 2.5$ between 59°N to 61°N and 139°W to 144°W. The dashed rectangles indicate the surge reservoir in the Bagley Ice Field and the surge receiving region of the Bering Glacier terminus. (a) Earthquakes (79) of $M_L \geq 2.5$ from August 1, 1990 through February 28, 1993. (b) Earthquakes (75) of $M_L \geq 2.5$ from March 1, 1993, through September 30, 1995. (c) Earthquakes (75) of $M_L \geq 2.5$ from October 1, 1995, through April 30, 1998. The earthquake data are from the National Earthquake Information Center earthquake database (`//gldss7.cr.usgs.gov/neis/epic/epic.html`).

Figure 10. Earthquakes of $M_L \geq 4.0$ from 1973 through 1997 between 59°N to 61°N and 139°W to 144°W. The largest earthquake to occur during this time period was a M_S=7.2 in February 1979 and the aftershocks associated with this event to dominate the seismicity pattern.

Table 1. Horizontal Site Velocities in a North American Fixed ITRF96 Reference Frame and Vertical Velocities Relative to Cape Yakataga

Station	Abbreviation	Latitude,°N	Longitude,°W	1993[a,b]	1995[a,b]	1997[a,b]	North, (mm/yr) ± 1σ	East, (mm/yr) ± 1σ	Vertical, (mm/yr) ± 1σ
				Icy Bay Region					
Amber	AMBR	60.006	-141.477	1	5	3	24.3 ± 1.8	-17.8 ± 2.2	11.7 ± 8.1
				Cape Yakataga Region					
White	WHTA	60.048	-142.066	1	7	0	31.5 ± 1.8	-19.0 ± 2.2	-4.7 ± 13.5
Cape Yakataga	VYAK	60.081	-142.486	7	12	9	30.5 ± 1.4	-15.8 ± 2.0	0 (reference site)
Yakataga USGS	YAKU	60.081	-142.508	5	3	3	30.6 ± 1.6	-17.1 ± 2.0	-1.5 ± 4.8
				Sites Near Surge Reservoir Region					
Anchor Ecc.	ANCX	60.442	-142.596	8	7	0	16.3 ± 1.6	-8.8 ± 2.0	26.3 ± 5.4
Isle	ISLE	60.601	-142.341	8	6	0	24.2 ± 1.6	-7.0 ± 2.0	29.9 ± 5.7
Time	TIME	60.774	-142.705	5	6	0	15.3 ± 1.6	-6.4 ± 2.2	18.2 ± 6.6
				Bering Glacier Region					
Don	DON	60.058	-143.376	2	6	-	7.4 ± 1.6	-17.1 ± 2.0	-21.0 ± 6.0
Don	DON	60.058	-143.376	-	6	4	31.9 ± 1.8	-18.0 ± 2.2	0.6 ± 7.8

[a]Number of observation days, most with 24 hours but some with 3-8 hours, especially in 1993.
[b]A dash means observations from that year were not included in the estimation of the deformation rate.

Table 2. Observed Versus Predicted Vertical Displacements(Millimeters), 1993–1995

Station Name	Vertical[a] Predicted	Vertical[b] Observed	North[a] Predicted	North[b] Observed	East[a] Predicted	East[b] Observed
DON	-42.0	-42.0	12.0	-49.0	-5.5	1.8
ANCX	35.4	32.6	-10.5	-15.0	1.5	13.4
ISLE	38.0	37.8	7.4	8.8	4.1	11.8
TIME	20.4	22.6	5.5	-3.2	-4.0	8.4
VYAK	3.7	0.0	-1.3	-0.2	-3.1	0.0

[a]Displacement predicted due to the loading/unloading disk distribution given in Plate 1.
[b]Total displacement estimated from GPS observations made in 1993 and 1995 minus the tectonic strain associated with subduction of the Pacific plate beneath interior Alaska.

Table 3. Constraints on Recent Ice Thinning Indicated by Height Differences Between Glacial Deposits and Nearby Glaciers

Location	Latitude, °N	Longitude, °W	Elevation, m	Height Change[a]	Method
Site 1: Guyot Glacier	60.02	141.47	305	305	moraine and overriden forest
Site 2: Malaspina Glacier	60.08	140.99	732	163+	lateral moraine at Chaix Hills
Site 3: Malaspina Glacier	60.13	140.61	610	137	lateral moraine at Samovar Hills
Site 4: Tyndall/Libbey Glacier	60.13	141.30	1006	762+	erratic boulders on ridge top
Site 5: Tyndall/Libbey Glacier	60.11	141.32	762	700+	erratic boulders on ridge top
Site 6: Tyndall/Libbey Glacier	60.31	141.15	610	500+	erratic boulders on ridge top
Site 7: Libbey Glacier	60.19	141.09	1067	300+	erratic boulders on ridge top
Site 8: Libbey Glacier	60.15	141.33	1006	365+	erratic boulders on ridge top
Site 9: Libbey Glacier	60.14	141.08	884	335+	erratic boulders on ridge top
Site 10: Libbey Glacier	60.13	141.10	823	275+	erratic boulders on ridge top
Site 11: Libbey Glacier	60.20	140.86	1219	120+	erratic boulders on ridge top
Site 12: Bagley Icefield	60.33	142.33	1128	90+	lateral moraine near Tana Glacier
Site 13: Jefferies Glacier	60.75	141.53	1768	27+	lateral moraine
Site 14: Bering Glacier	60.10	143.50	91	180	since 1967

Sites 1–12 are from unpublished data by G. Plafker; site 13 from unpublished data by J. Sauber; site 14 from *Molnia and Post* [1995].

[a]Height change is from highest recent glacial deposits to the nearby glacial level. For stations 1–13 the height difference was estimated by a helicopter altimeter and are estimated to be ± 15 m. For stations 1–11 the elevations of the glacial deposits are inferred to approximate the most recent glacial maximum in about 1900 (*Plafker and Miller*, [1958]). For station 12 and 13 deposits are of unknown age but may correspond to the 1900 maximum.

Table 4. Observed Versus Predicted Displacement Rates at AMBR relative to Cape Yakataga

Type	North	East	Vertical
Observed rate	6.2	2.0	11.7
Predicted tectonic	±5	±5	±5
Predicted annual	0.7	0.0	3.1
5×10^{20} Pa s	0.1	0	1.4
5×10^{19} Pa s	0.6	0	9.3
5×10^{18} Pa s	1.6	0	31.2

Units are millimeter per year.

Table 5. Selected Radiocarbon Ages for Marine Terraces at Icy Bay [*Plafker et al.*, 1981] and Vitus Lake [*Molnia and Post*, 1995]

Lab. No.	Latitude, Longitude	Carbon14 Age[a]	Calendar Age[b]	Net Uplift[c]	Uplift Rate[d]	Location
W-4728	60.08°N, 143.258°W	1300 ± 40	1389–967 Midrange: 1198	17.8	15 (1198–0 years B.P.)	Icy Bay terrace III
W-4485	60.088°N, 142.258°W	2450 ± 80	2744–2329 Midrange: 2533	27.8	8 (2533–1198 years B.P.)	Icy Bay terrace II
W-4495	60.138°N, 141.908°W	4990 ± 90	5919–5586 Midrange: 5712	60.6	10 (5712–2533 years B P.)	Icy Bay terrace I
W-6499	60.088°N, 143.608°W	4860 ± 80	5660–5491 Midrange: 5597	13.5	2 (5597–0 years B.P.)	uplifted shoreline near Vitus Lake at Bering Glacier

[a]Years before present.
[b]Range in years before present; calendar age (2σ) from *Stuiver and Reimer* [1993] calibration.
[c]Meters; assumes an average late Holocene sea level rise of 1.5 mm/yr [*Bard et al.*, 1990].
[d]Millimeters per year, calculated from the midrange calendar age.

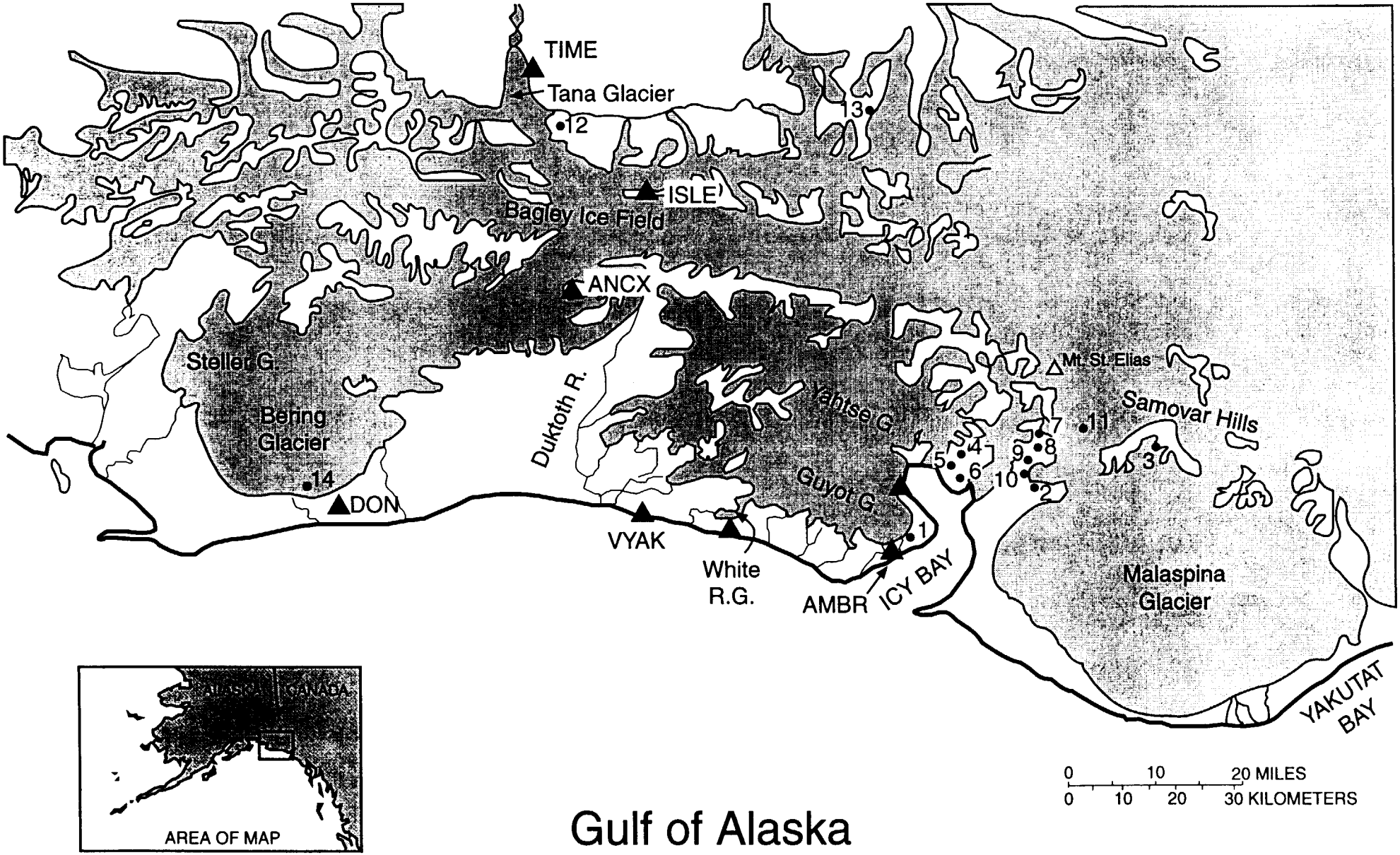

Gulf of Alaska

Fig 1

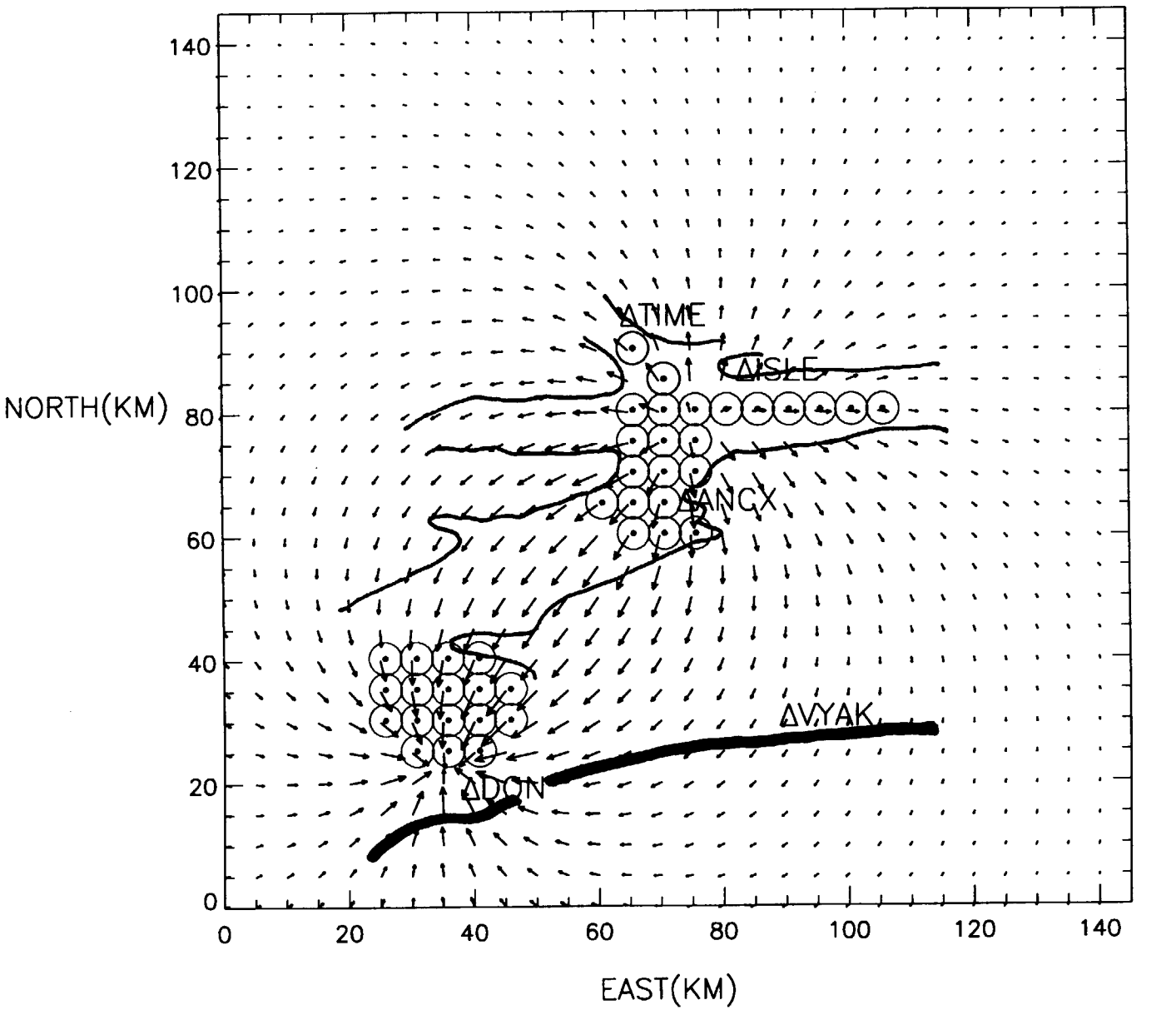
140
120
100
80
60
40
20
0
NORTH(KM)
0
20
40
60
80
100
120
140
EAST(KM)
ATIME
AISLE
ANCX
AVYAK
ADON
15 mm

Plate 1

Plate 2

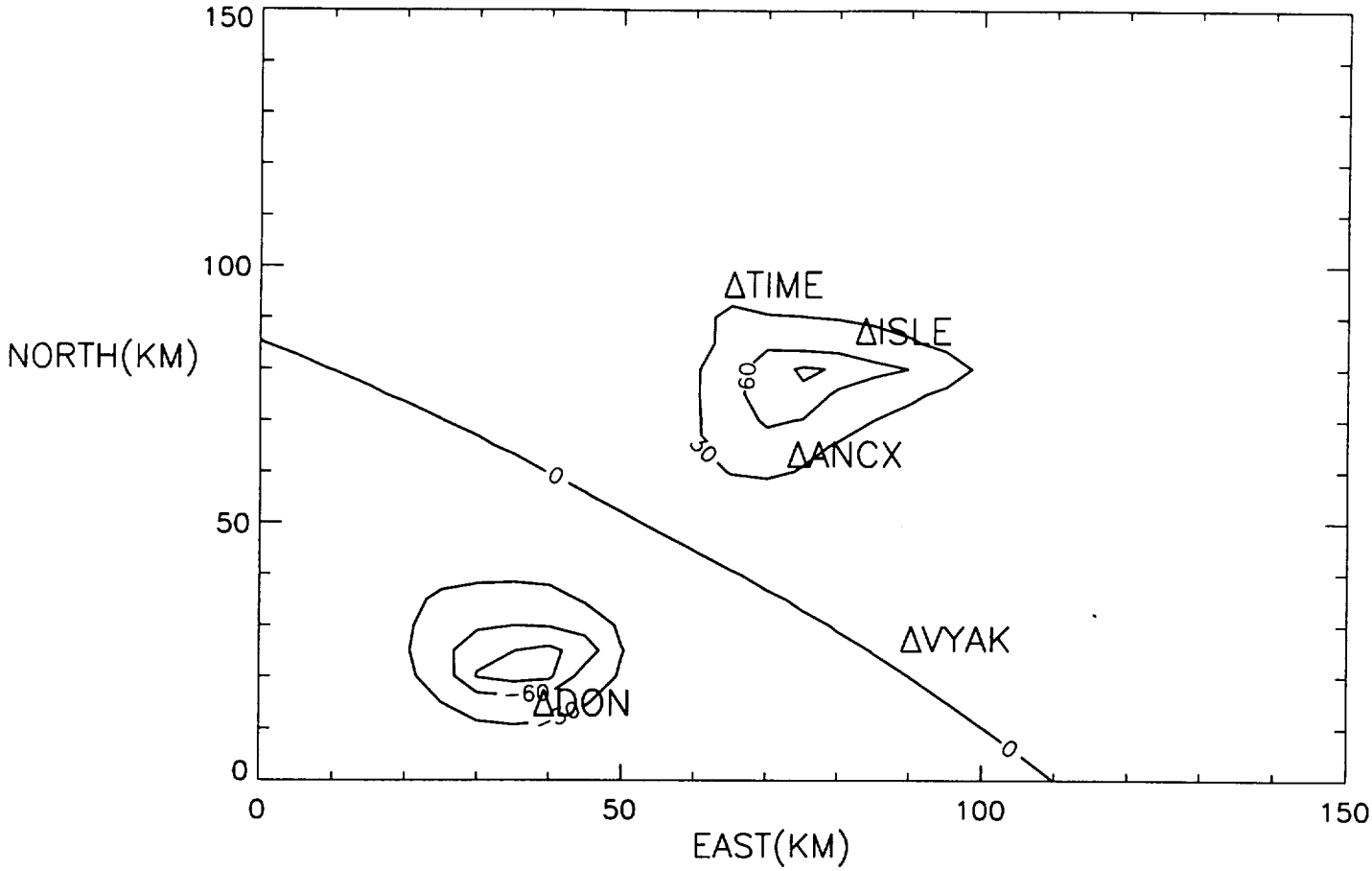
150
100
50
0
NORTH(KM)
0
50
100
150
EAST(KM)
ΔTIME
ΔISLE
ΔANCX
ΔVYAK
ΔDON
60
30
0
0
-60

Fig 2

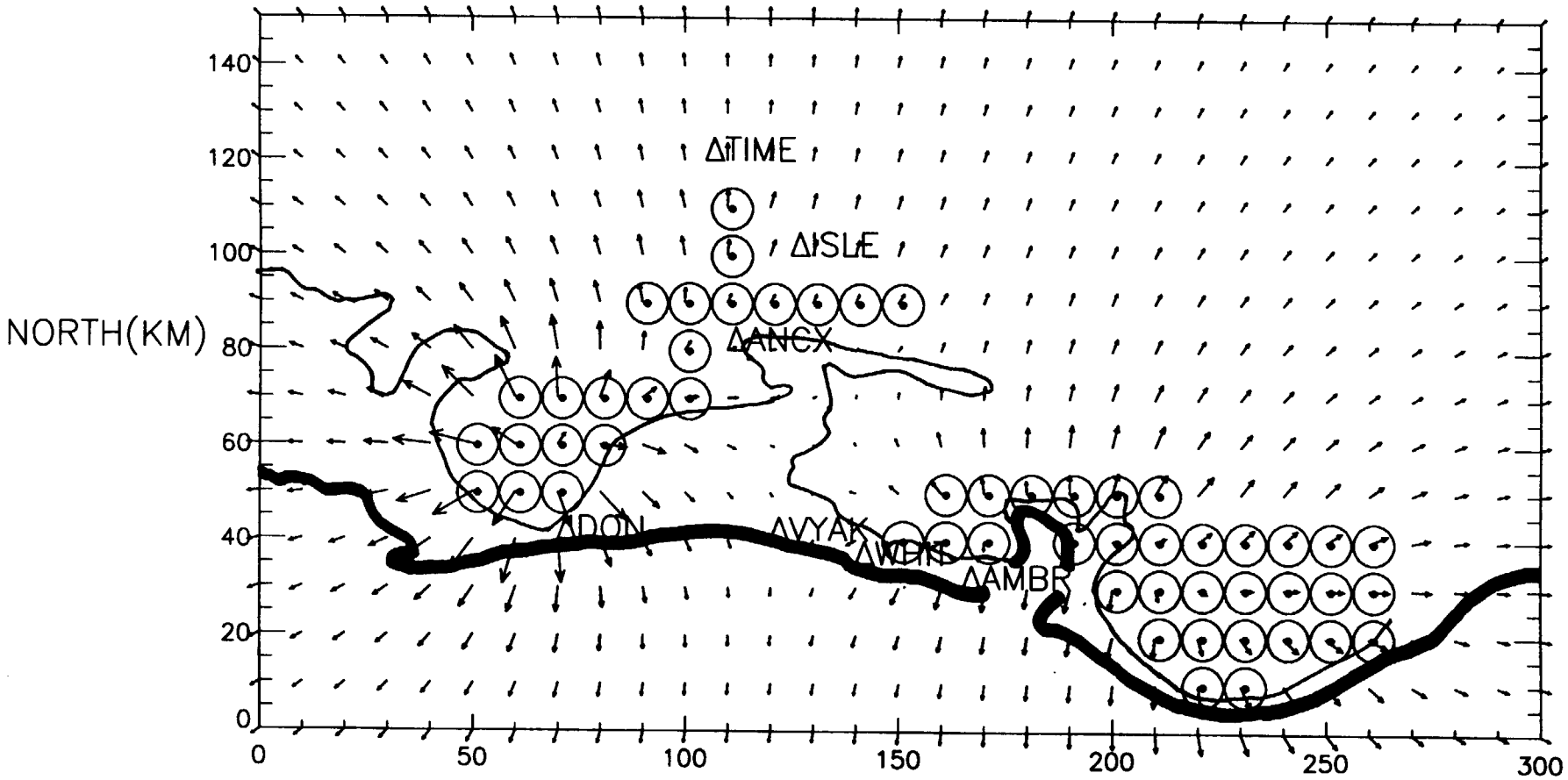
ΔiTIME
ΔISLE
ΔANCX
ΔDON
ΔVYAK
ΔWRH
ΔAMBR
NORTH(KM)
EAST(KM)
0
20
40
60
80
100
120
140
0
50
100
150
200
250
300
2 mm

Fig 3

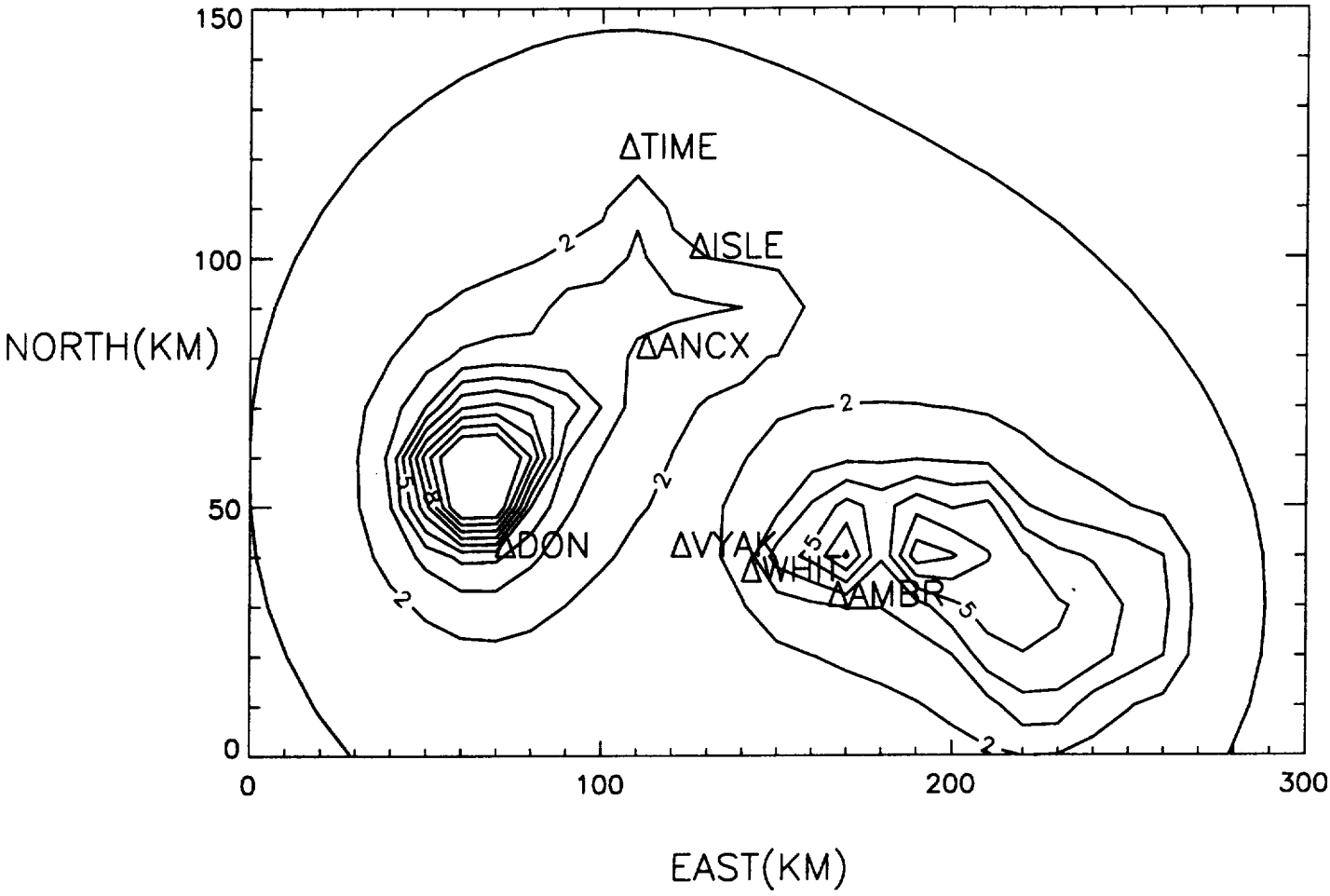
150
100
50
0
NORTH(KM)
0
100
200
300
EAST(KM)
ΔTIME
ΔISLE
ΔANCX
ΔDON
ΔVYAK
ΔWHIT
ΔAMBR
2
5

Fig 4

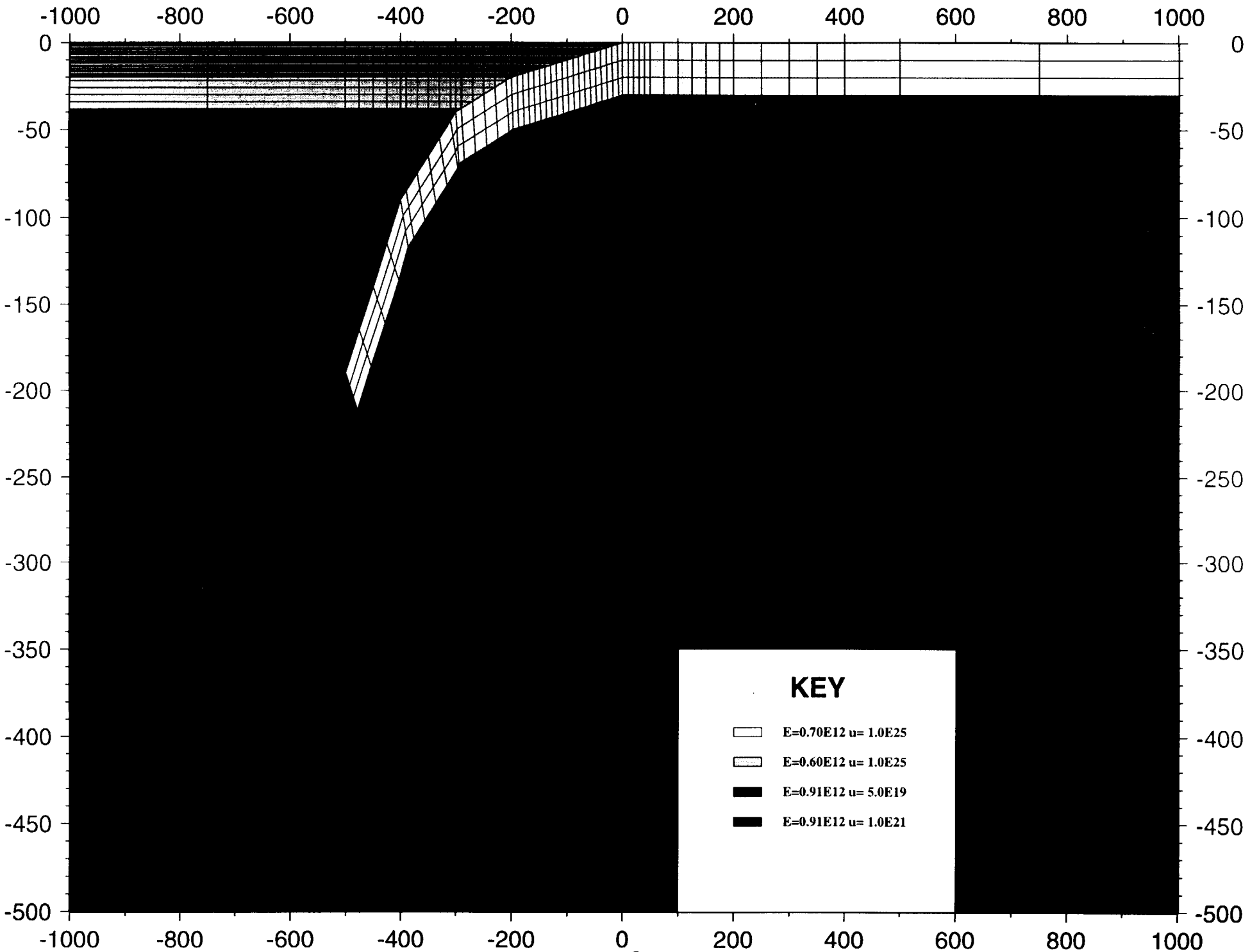
-1000
-800
-600
-400
-200
0
200
400
600
800
1000
0
-50
-100
-150
-200
-250
-300
-350
-400
-450
-500
KEY
E=0.70E12 u= 1.0E25
E=0.60E12 u= 1.0E25
E=0.91E12 u= 5.0E19
E=0.91E12 u= 1.0E21

Fig 5

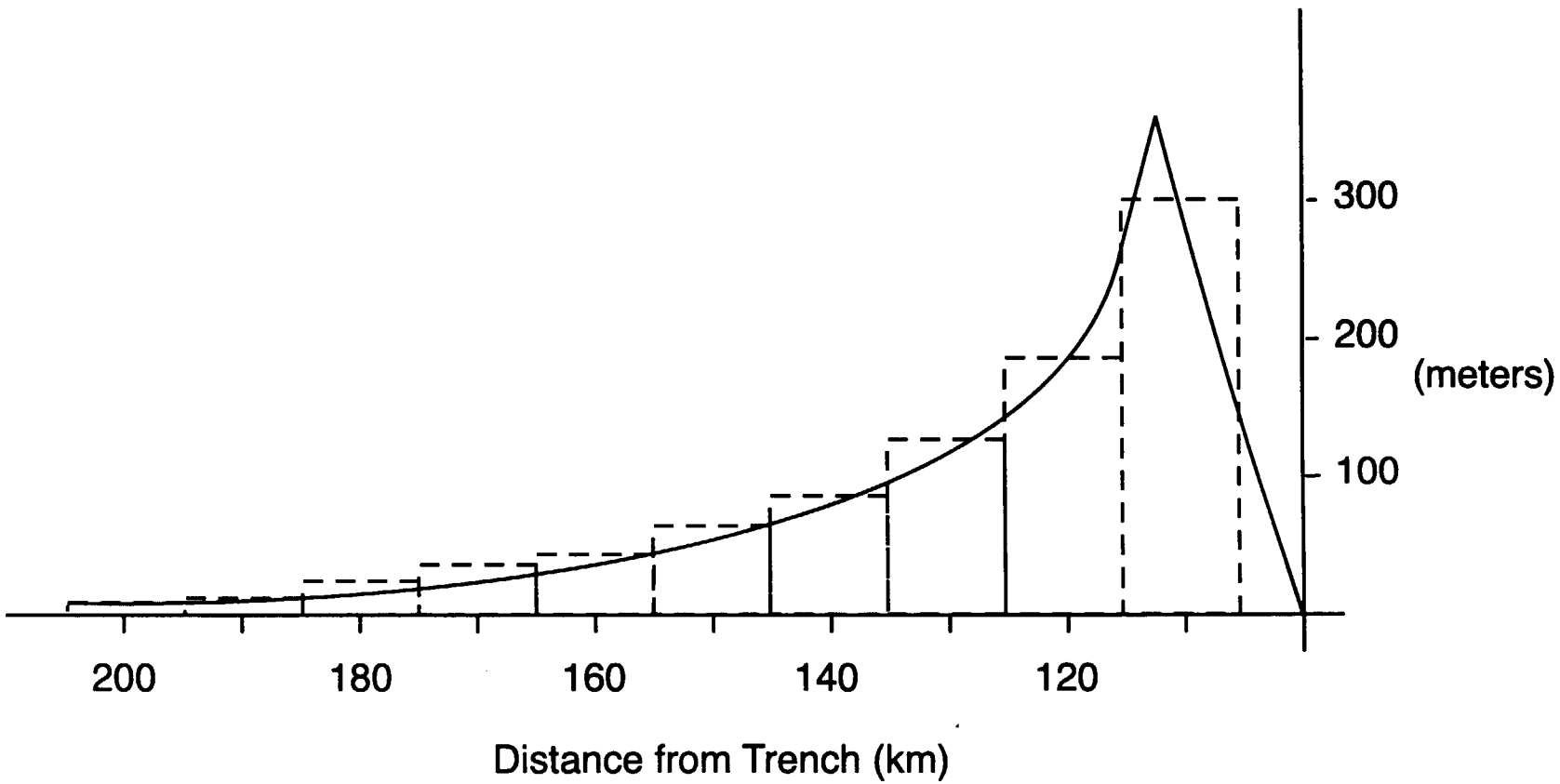
300
200
100
(meters)
200
180
160
140
120
Distance from Trench (km)

Fig 6

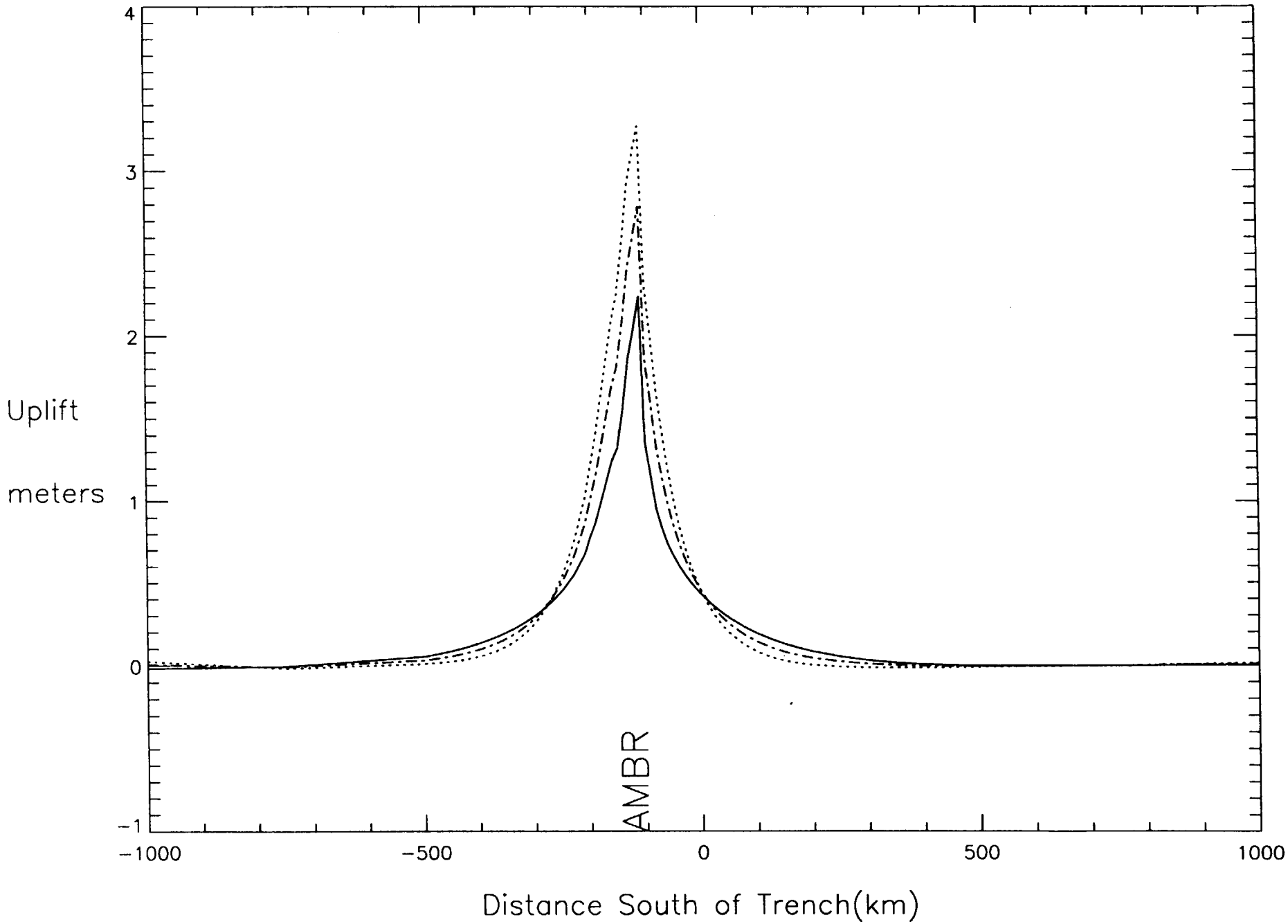
4
3
2
1
0
−1
Uplift
meters
AMBR
−1000
−500
0
500
1000
Distance South of Trench(km)

Fig 7a

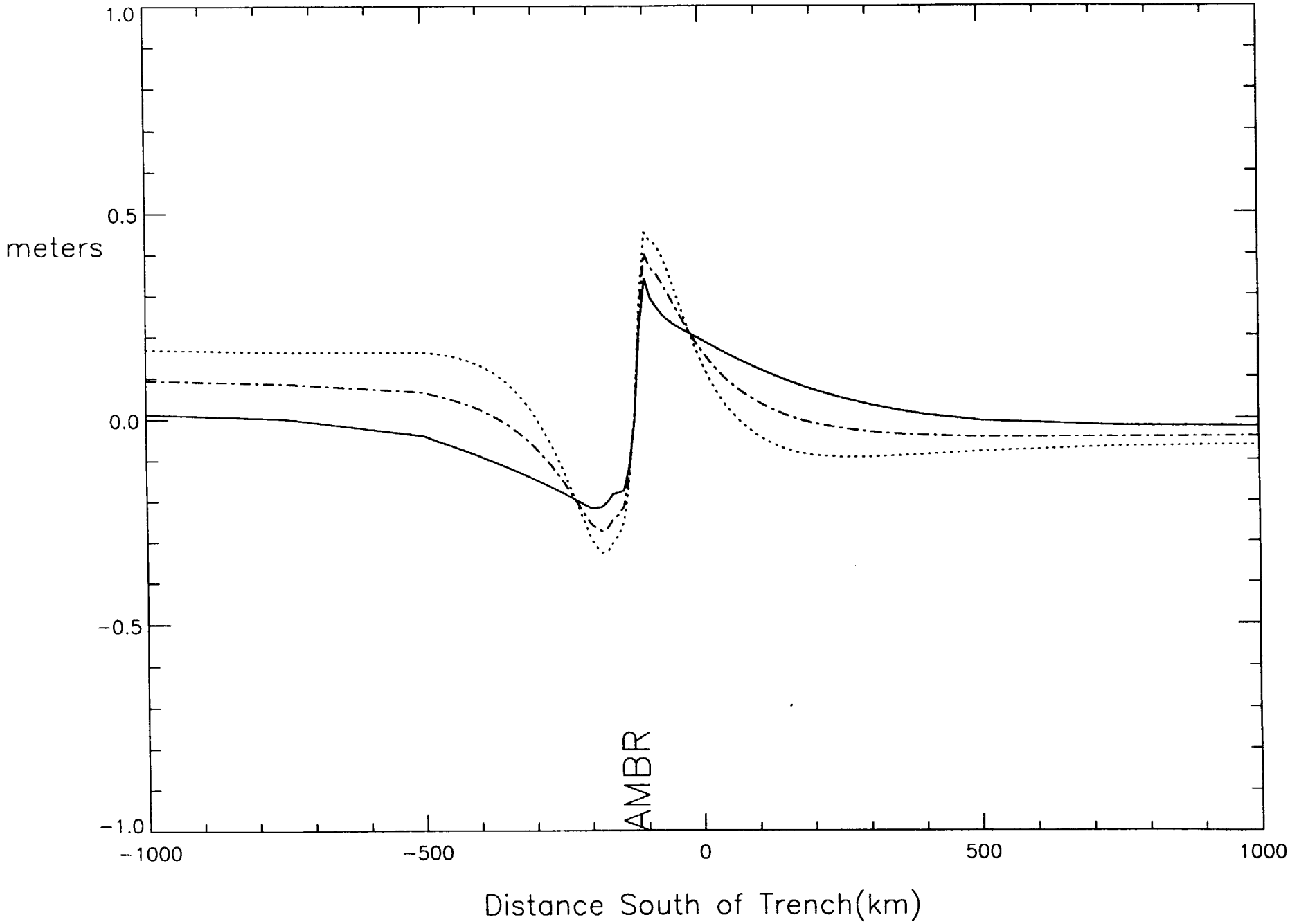
1.0
0.5
meters
0.0
−0.5
−1.0
−1000
−500
0
500
1000
AMBR
Distance South of Trench(km)

Fig 7b

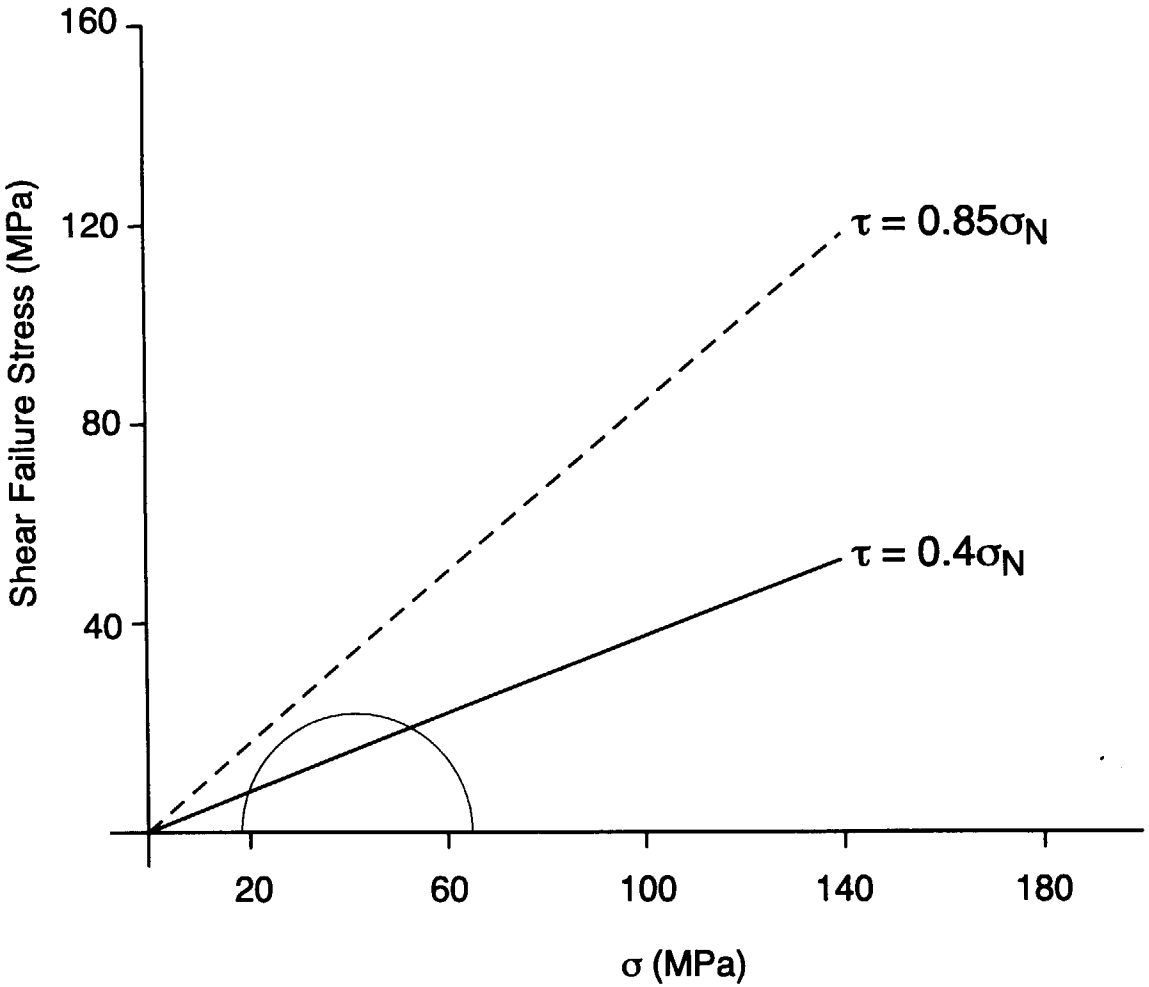

Stress Drop in Earthquakes

⊢⊣ 2 - 10 MPa

Sediment Loading (σ_v^E)

H ~1 MPa

Retreat (σ_v)

H 1 MPa

Surge (σ_v)

H 0.5 MPa

Fig 8

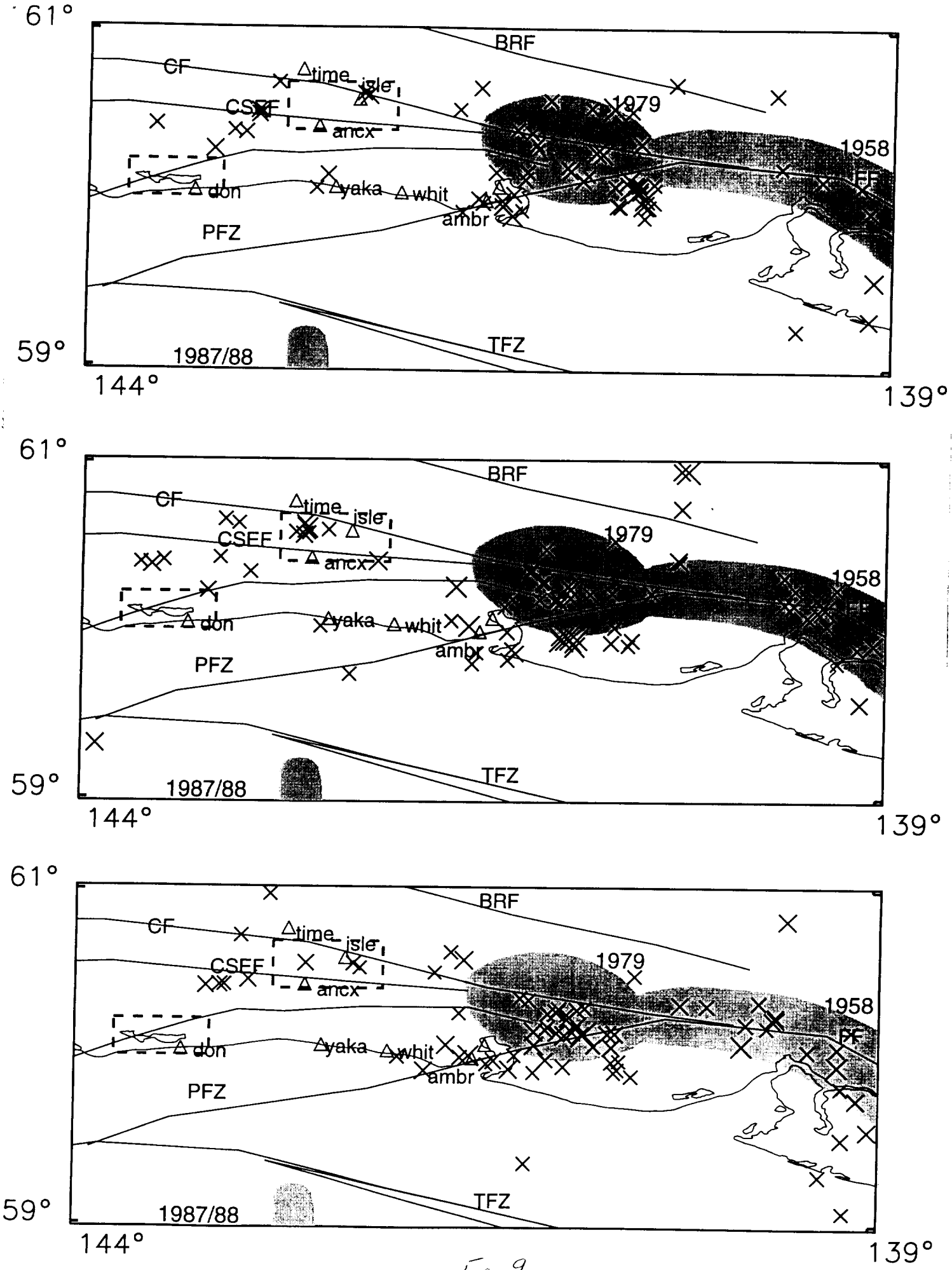
61°
BRF
CF
time
isle
CSEF
ancx
1979
1958
EF
don
yaka
whit
ambr
PFZ
TFZ
59°
1987/88
144°
139°
61°
BRF
CF
time
isle
CSEF
ancx
1979
1958
don
yaka
whit
ambr
PFZ
TFZ
59°
1987/88
144°
139°
61°
BRF
CF
time
isle
CSEF
ancx
1979
1958
PF
don
yaka
whit
ambr
PFZ
TFZ
59°
1987/88
144°
139°

Fig 9

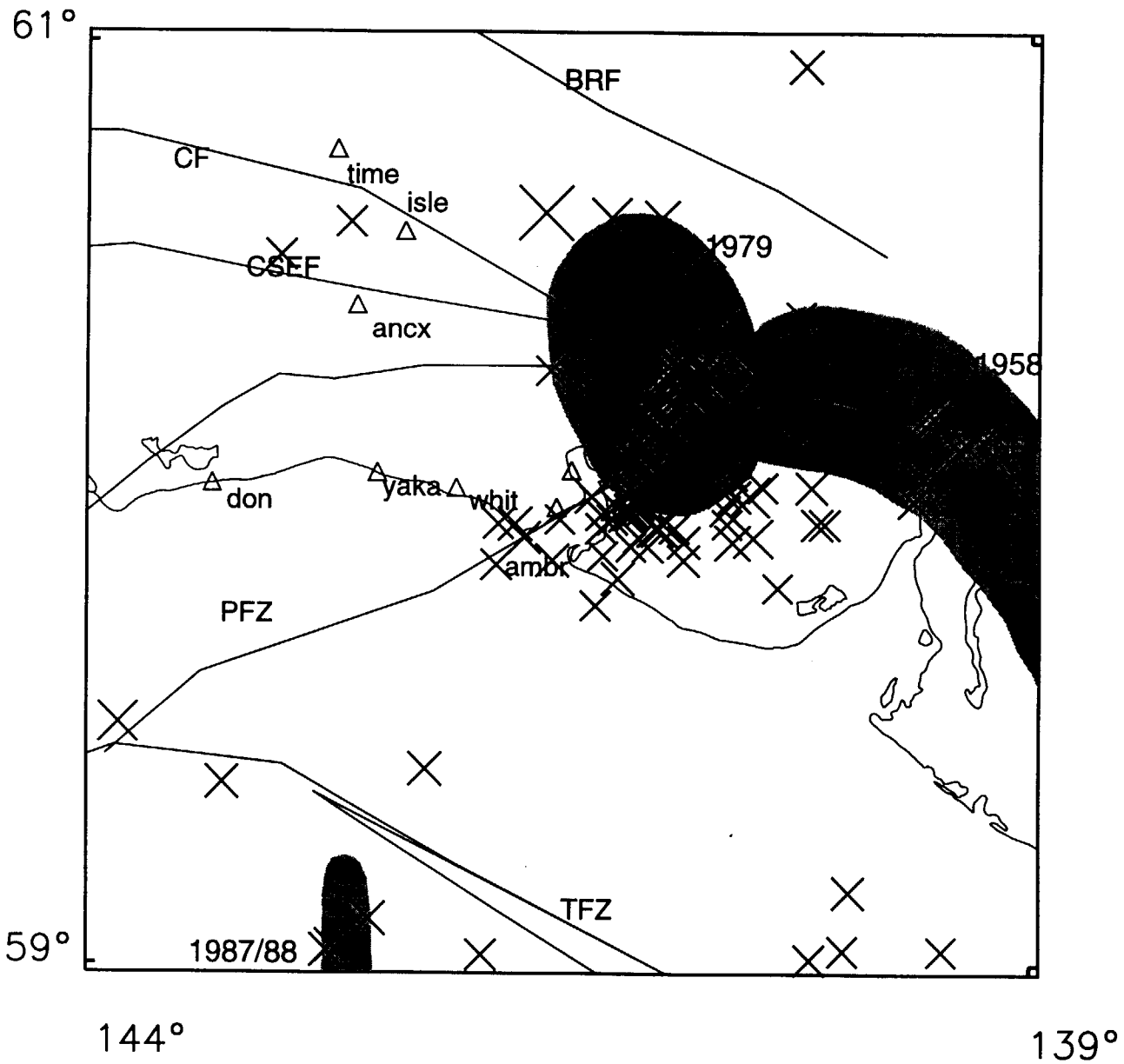
61°
BRF
CF
time
isle
CSEF
1979
ancx
1958
don
yaka
whit
ambr
PFZ
TFZ
1987/88
59°
144°
139°

Fig. 10